Universidade do Minho
Escola de Engenharia

Ana Catarina Sampaio Ribeiro

Exploring the role of Vav3 in the repair of toxin-induced plasma membrane damage

Dissertação de Mestrado

Mestrado Integrado em Engenharia Biológica

Trabalho efetuado sob a orientação da(s)

Doutora Sandra Sousa

Professora Doutorada Lucília Domingues

Janeiro de 2021

DIREITOS DE AUTOR E CONDIÇÕES DE UTILIZAÇÃO DO TRABALHO POR TERCEIROS

Este é um trabalho académico que pode ser utilizado por terceiros desde que respeitadas as regras e boas práticas internacionalmente aceites, no que concerne aos direitos de autor e direitos conexos.

Assim, o presente trabalho pode ser utilizado nos termos previstos na licença abaixo indicada. Caso o utilizador necessite de permissão para poder fazer um uso do trabalho em condições não previstas no licenciamento indicado, deverá contactar o autor, através do RepositóriUM da Universidade do Minho.

Licença concedida aos utilizadores deste trabalho

Atribuição-NãoComercial-SemDerivações
CC BY-NC-ND
https://creativecommons.org/licenses/by-nc-nd/4.0/

Agradecimentos

Quero aproveitar o término da dissertação para agradecer a todas as pessoas que direta ou indiretamente me ajudaram a conquistar mais uma etapa. O mais sincero obrigada aos professores que me acompanharam nestes cinco anos de crescimento.

À Professora Lucília Domingues por toda a ajuda, disponibilidade e ensinamentos ao longo do meu percurso académico como docente de engenharia biológica.

Um agradecimento especial à Doutora Sandra não só pela oportunidade que me proporcionou ao aceitar-me no seu grupo de investigação "*Cell Biology of Bacteria Infections*", mas também pela orientação, experiência transmitida, conhecimento e principalmente por toda a disponibilidade e acompanhamento ao longo do estágio.

Agradeço ao Doutor Didier Cabanes por toda a boa disposição, orientação, conhecimento e principalmente por todas as questões que me faz nos lab meetings, que me permitem ter uma nova perspetiva do trabalho e vontade de continuar a evoluir.

Um sincero obrigada, à Joana Pereira por toda a ajuda, partilha de conhecimento, orientação, amizade e motivação. Agradeço também pelo carinho e por toda a disponibilidade em me acompanhar, especialmente na fase inicial, e principalmente, por toda a paciência ao longo do projeto.

Agradeço à Doutora Rita Pombinho toda a orientação, ajuda, partilha de conhecimento e paciência na elaboração dos constructos bem como na realização do RT-PCR.

Não posso deixar de agradecer a todos os meus colegas de laboratório (Diana, Ricardo, Sara, Alexandra e Lua) por toda a interajuda, companheirismo, boa disposição e troca de conhecimento.

Agradeço do fundo do coração à minha família por todo o apoio e amor incondicional, compreensão e sacrifício para que sempre pudesse realizar os meus sonhos.

Aos meus amigos, deixo o meu muito obrigada, por todo o carinho, amizade e motivação que sempre me ofereceram.

STATEMENT OF INTEGRITY

I hereby declare having conducted this academic work with integrity. I confirm that I have not used plagiarism or any form of undue use of information or falsification of results along the process leading to its elaboration.

I further declare that I have fully acknowledged the Code of Ethical Conduct of the University of Minho.

Resumo

A saúde e o bem-estar de uma célula dependem diretamente da integridade da sua membrana plasmática (PM) e da sua capacidade em repará-la após eventos de rutura que ameaçam as células individuais e organismos multicelulares induzindo a morte celular e a inflamação dos tecidos. As bactérias patogénicas produzem e secretam poderosos fatores de virulência, como toxinas formadoras de poros (PFTs) que, uma vez secretadas pela bactéria, difundem-se em direção à célula-alvo, à qual se ligam por meio de um recetor específico formando poros na PM. As proteínas do citoesqueleto e da matriz extracelular são responsáveis por conferir resistência aos danos da PM. Além disso, as proteínas do citoesqueleto modulam as propriedades intrínsecas da PM conferindo resistência às lesões, representando, assim, um mecanismo preventivo contra danos da membrana.

A listeriolisina O (LLO) é uma toxina formadora de poros dependente do colesterol, produzida pela *Listeria monocytogenes*, um patógeno bacteriano oportunista responsável pela doença listeriose. Esta doença começa com a ingestão de alimentos contaminados e afeta principalmente indivíduos imunocomprometidos, idosos, recém-nascidos e grávidas.

Esta dissertação foca-se no papel da Vav3, um regulador da dinâmica do citoesqueleto, nos mecanismos de reparação de danos da PM induzidos por toxinas. Para isso, células epiteliais humanas a expressar diferentes níveis de Vav3 foram intoxicadas com LLO purificada e os processos de dano e reparação foram avaliados por ensaios de permeabilização das células com iodeto de propídio. Além disso, as alterações na expressão de *vav3* após a intoxicação por LLO foram avaliadas por RT-qPCR. Os dados mostram que a sobrexpressão de Vav3 não representa uma vantagem durante a intoxicação com concentrações sub-líticas de LLO e as células não aumentam a expressão de *vav3* após a intoxicação por LLO. No entanto, os resultados sugerem um possível papel para Vav3 em resposta a concentrações líticas de LLO. Essas observações precisam de ser exploradas sob uma forma experimental mais complexa, que é proposta aqui.

Palavras-Chave

LLO; membrana-plasmática; reparação de dano; toxinas-formadoras de poros; Vav3.

Abstract

Health and well-being of a cell critically depend on the integrity of its plasma membrane (PM) and its ability to repair itself upon critical PM disruption events that threat individual cells and multicellular organisms, inducing cell death and tissue inflammation. Pathogenic bacteria produce and secrete powerful virulence factors, such as pore forming toxins (PFTs) that once secreted by the bacteria, diffuse towards their target cell, to which they bind via a specific receptor forming PM pores. Proteins from the cytoskeleton and the extracellular matrix are main actors conferring resistance to the PM damage. In addition, cytoskeletal proteins modulate the intrinsic properties of the PM to confer resistance to wounds, thus representing a preventive mechanism against membrane injuries.

Listeriolysin O (LLO) is a cholesterol-dependent pore-forming toxin produced by *Listeria monocytogenes*, an opportunistic bacterial pathogen responsible for the disease listeriosis. This disease starts with the ingestion of contaminated foods and mainly affects immunocompromised individuals, elderly, newborns, and pregnant women.

This dissertation concentrates on the role of Vav3, a master regulator of cytoskeletal dynamics, in the repair mechanisms of toxin-induced PM damage. For this, human epithelial cells expressing different levels of Vav3 were intoxicated with purified LLO and the damage and repair processes were evaluated by propidium iodide permeabilization assays. In addition, changes in *vav3* expression upon LLO intoxication were assessed by RT-qPCR. Data show that Vav3 overexpression does not represent an advantage during intoxication with sub-lytic concentrations of LLO and cells do not increase *vav3* expression upon LLO intoxication. However, the results suggest a possible role for Vav3 in response to lytic concentrations of LLO. These observations need to be further explored under a more complex experimental setup, which is proposed here.

Keywords

Listeriolysin O; Plasma membrane damage; Pore-forming toxins; Repair of damage; Vav3.

Contents

Figure Index

Table Index

List of Abbreviation

Ac: Acid region

CDCs: Cholesterol-dependent cytolysins

CH: Calponin homology

DH: Dbl homology

FBS: Fetal bovine serum

GAPs: GTPase-activated proteins

GEFs: Guanine nucleotide exchange factors

GFP: Green fluorescent protein

LB: Lysogeny Broth

LLO: Listeriolysin O

Lm: Listeria monocytogenes

MCS: multicloning site

PBS: Phosphate buffer solution

PCR: Polymerase Chain Reaction

PFTs: Pore-forming toxins

PH: Pleckstrin homology

PI: Propidium iodide

PM: Plasma membrane

Small GTPases: Small GTP-hydrolyzing enzymes

ZF: Zinc finger

1. INTRODUCTION

1.1 Pore-forming toxins

Pore-forming toxins (PFTs) are sophisticated and widely spread virulence factors produced by a variety of human bacterial pathogens (Table 1). They are the biggest class of bacterial toxins and integrate a major class of pore-forming proteins[1]. PFTs comprise 25 % to 30 % of cytotoxic bacterial proteins. During infection, PFTs act by disrupting epithelial barriers allowing evasion of host immune responses, causing organism threat and concomitant bacterial growth and dissemination[2].

Table 1. Bacterial pore-forming toxin (PFT), pathogen, receptor and toxin type

Toxin	Pathogen	Receptor	Toxin Type	Ref
Aerolysin	*Aeromonas hydrophila*	GPI-APs	Small β-PFT	[3]
α-toxin	*Staphylococcus aureus*	Lipid clusters	Small β-PFT	[4]
α-toxin	*Clostridium septicum*	GPI-APs	Small β-PFT	[5]
Cry5B	*Bacillus thuringiensis*	GPI-Aps, glycolipids, lipids	Small α-PFT	[6]
Streptolysin O (SLO)	*Streptococcus pyogenes*	Lipid/cholesterol	CDCs (β-PFT)	[7]
Listeriolysin O (LLO)	*Listeria monocytogenes*	Lipid/cholesterol	CDCs (β-PFT)	[8]
Pneumolysin O (PLY)	*Streptococcus pneumoniae*	Lipid/cholesterol	CDCs (β-PFT)	[8]
Perfringolysin O (PFO)	*Clostridium perfringens*	Lipid/cholesterol	CDCs (β-PFT)	[8]
Anthrax toxin	*Bacillus anthracis*	CMG2, TEM8	AB/Small β-PFT	[9,10]
Vcc	*Vibrio cholerae*	Carbohydrate receptors	Small β-PFT	[11]
Colicin Ia	*Escherichia coli*	Cir	α-PFTs	[12]
Pyolysin	*Arcanobacterium pyogenes*	Cholesterol	β-PFTs	[13]

Toxin	Pathogen	Receptor	Toxin Type	Ref
Anthrolysin O (ALO)	*Bacillus anthracis*	Cholesterol	CDCs (β-PFTs)	[14]
Botulinolysin	*Clostridium botulinum*	Cholesterol	β-PFTs	[15]
Tetanolysin	*Clostridium tetani*	Cholesterol	β-PFTs	[16]
Vaginolysin	*Gardnerella vaginalis*	CD59/cholesterol	β-PFTs	[17]
Ivanolysin	*Listeria ivanovii*	Cholesterol	β-PFTs	[18]

Monomers of PFTs are secreted to the extracellular milieu and interact with the host plasma membrane (PM) through a variety of receptors that range from sugar moieties, protein receptors to specific lipid sterols[19]. PM bound monomers oligomerize and insert into the host PM creating a pore (Figure 1). The cholesterol-dependent cytolysins (CDCs)[8,20], which specifically recognize and bind cholesterol at the host cell PM, oligomerize to form a huge structure named pre-pore, which assembles at the host PM but do not disrupt its integrity (Figure 1). PM insertion of the pre-pore leads to the formation of a large transmembrane pore, which allows the uncontrolled influx and efflux of ions, small molecules and proteins (Figure 1), and triggers the activation of various secondary responses involved in programmed cell death pathways or in repair mechanisms[1,21].

Distinct PFTs form pores with specific sizes and biophysical properties, which in turn induce different phenotypes and responses in target cells[1]. PFTs can be classified into two large class - α-PFTs and β-PFTs - based on whether the secondary structure of their membrane-spanning region is composed of α-helices or β-barrels, respectively[12]. Six families of PFT have been identify based on their structure: three families of α-PFTs and three families of β-PFTs[1].

This dissertation focuses on a particular PFT, which is named Listeriolysin O (LLO) and is produced by the human pathogen *Listeria monocytogenes*.

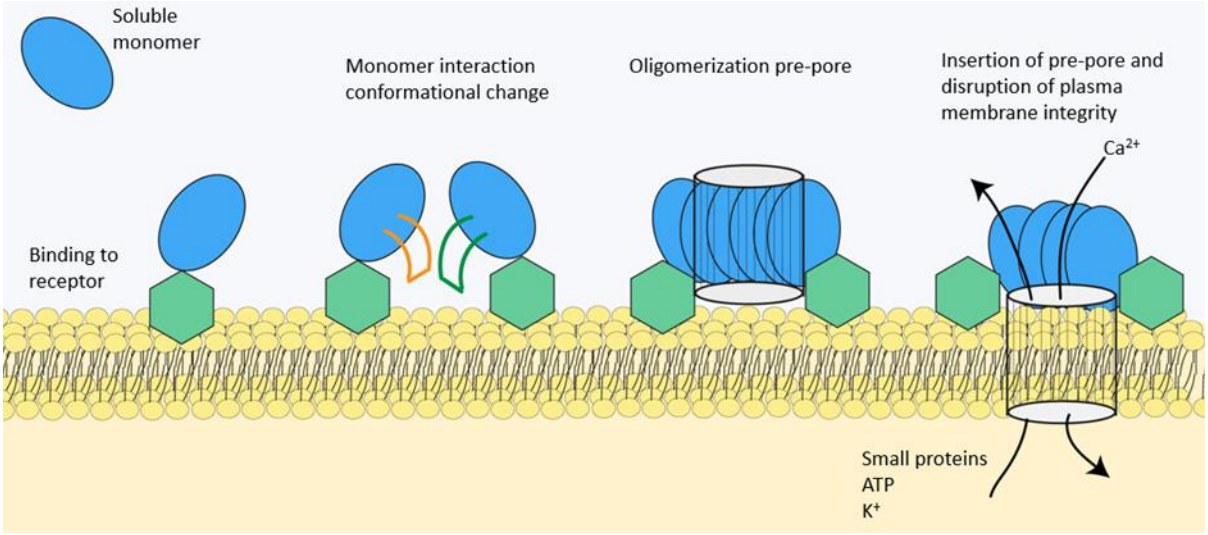

Figure 1. Schematic representation of the pore assembly pathway of pore-forming toxins (PFTs)[1]. PFTs are secreted by pathogens as soluble monomers which interact with the host PM via interaction with specific receptors, oligomerize and insert into host PM disrupting cellular integrity. The large-pore-forming cholesterol-dependent cytolysins are characterized by their ability to first bind to the PM cholesterol, assemble into pre-pore structure which upon insertion in the PM form large and permeable transmembrane pores allowing the uncontrolled flux of molecules (ions, proteins, ATP, etc) across the PM. The free exchanges between the extracellular and intracellular environments severely compromise cell fate, to survive damaged cells need to rapidly repair the PM pore and restore PM selective permeability.

1.2 *Listeria monocytogenes* and its pore-forming toxin, Listeriolysin O

Listeria monocytogenes (*Lm*) is an opportunistic Gram-positive human pathogen first described in 1926 upon an epidemic outbreak that affected rabbits and guinea pigs[22]. It was recognized as a cause of significant human diseases during the second world war, when several cases of neonatal sepsis and meningitis have been documented[23]. *Lm* became best known in immunocompromised adults in the 1950s and 1960s due to the introduction of chemotherapeutic agents[24]. However, it was only in 1981, after a severe outbreak[25] that *Lm* emerged as a foodborne bacterial pathogen responsible for a multiparameter disease named listeriosis[26], which mainly affects immunocompromised individuals, elderly, newborns and pregnant women[27]. While in healthy humans listeriosis mainly manifests as gastroenteritis, in individuals of risk groups *Lm* infection causes meningitis, septicemia, abortions, stillbirth, among others[28].

Lm is a facultative intracellular pathogen, it is widespread in the environment and is commonly found in water, soil and vegetation[29]. This bacterium is particularly well adapted to

harsh environmental conditions and can thus resist and grow under high stress[22] such as low temperature, high salt concentrations and low pH[25]. Given that this conditions are normally used for food conservation, *Lm* is a major concern for food industry[29].

Human infection occurs upon the ingestion of contaminated food (such as deli meat, vegetables and dairy products) by the host[30]. Following ingestion, *Lm* has the capacity to overcome harsh gastric conditions, and reaches the lumen of the intestine where it interacts with the intestinal epithelium. *Lm* has the ability to invade the cells from the intestinal epithelium, traverses the intestinal epithelial barrier and then disseminates via the lymph and blood towards its target organs, the liver and the spleen[22,29–31]. It can then cross the blood–brain barrier in immunocompromised individuals or the fetoplacental barrier in pregnant women thus reaching the central nervous system or the fetus, respectively (Figure 2).

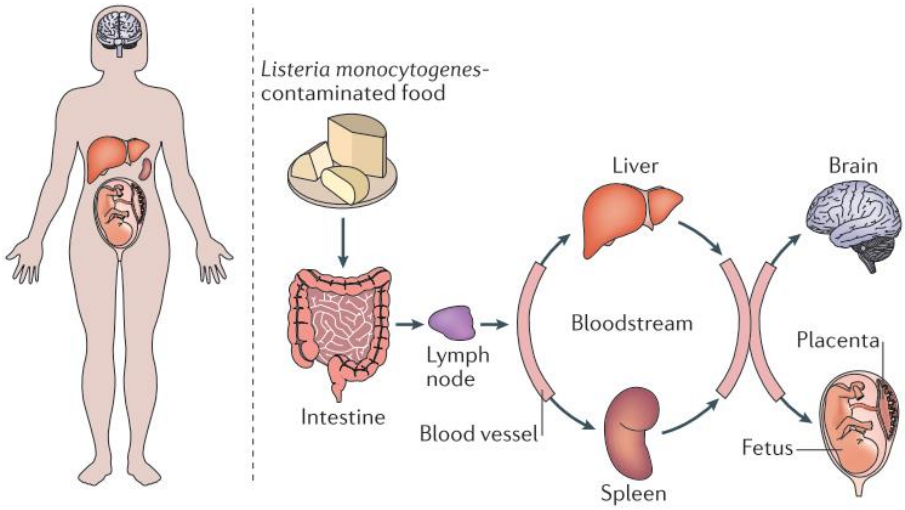

Figure 2. Schematic representation of the successive steps of *Listeria monocytogenes* infection in humans, after ingestion of contaminated food. Adapted from from Radoshevich and Cossart, 2017 [22].

The infectious cycle of *Lm* strongly depends on its capacity to invade, survive and replicate inside a variety of host cell types[32]. The cycle of cellular infection by *Lm* is known in great detail[33] (Figure 3). A variety of virulence factors was described and their specific functions during cellular infection were extensively studied during the last decades. *Lm* express surface proteins that recognize and interact with specific receptors at the surface of host cells, mimicking their natural ligands. Through these protein-protein interactions *Lm* triggers intracellular signaling cascades inducing its own uptake by receptor-mediated phagocytosis[34]. *Lm* thus reaches the intracytoplasmic environment entrapped in a phagosome, which is destabilized by the expression and secretion of LLO, a PFT that allows

bacterial escape from the internalization vacuole. Cytosolic bacteria rapidly replicate and induce the polymerization of the host cell's actin at one pole (Figure 3). This actin tail propels the bacteria through the host cell cytosol, allowing the invasion of neighboring cells, in which *Lm* is trapped in a double-membrane vacuole that is disrupted also by the mean of LLO. In this newly infected cell a new infection cycle is started[21] (Figure 3).

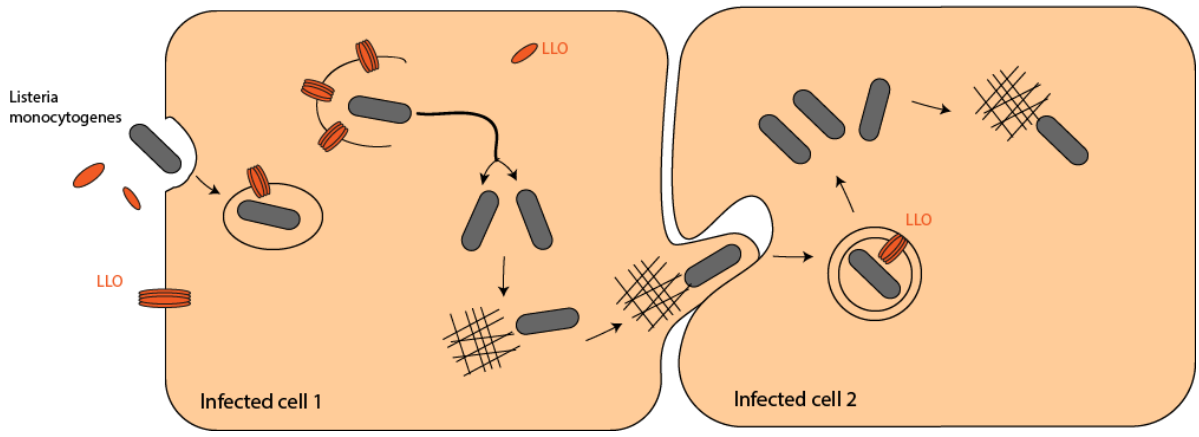

Figure 3. Schematic representation of intracellular infection cycle of *L. monocytogenes* and its cell-to-cell spread. *Lm* started to adhere to cells and then it induces its own internalization in cell 1. *Lm* is entrapped in a phagosome which it destabilizes by expressing LLO which disrupts the vacuole and allows bacterial escape. Intracellular LLO seems to be rapidly degraded to avoid inside-out damaging of host cell membranes. Cytosolic bacteria replicate and induce host cell actin polymerization (represent by the cross dash) to propel the bacterium across the cytosol allowing spread to cell 2. There, *Lm* is entrapped in a double-membrane vacuole, engaging LLO expression and possibly additional molecular mechanisms to disrupt it and start the intracellular replication cycle again[21].

LLO is thus a crucial virulence factor that mediates the escape of *Lm* from the phagocytic vacuole, avoiding lysosome fusion and killing by lysosomal enzymes, and enabling bacterial replication into the host cell cytoplasm[32,33]. Confirming the critical role of LLO in the infection, while the wild-type bacteria rapidly escape from the internalization vacuole and multiply in the host cytosol, LLO-deficient mutants are retained in the vacuole, have limited intracellular growth and are avirulent in animal infection models of listeriosis[33].

LLO is a *Lm* secreted toxin that belongs to CDC superfamily and is classified as a β-PFT. It distinguishes from other CDC family members by having a pH regulated activity[1,21]. The ideal pH for LLO activity is 5.5, suggesting that it has adapted to the specific setting of the acidified phagosome[26] to promote its efficient disruption and the consequent release of the bacteria into the host cell cytoplasm. Intracellular LLO appears to be rapidly degraded to prevent inside-out damage of host cell membranes[35]. Besides its intracellular role in the disruption of

the phagocytic vacuole, LLO water-soluble monomers produced by extracellular bacteria bind cholesterol and oligomerize at the PM of target cells[21,36]. PM insertion of LLO results in transmembrane stable pores that lead to increased PM permeability and allow uncontrolled exchanges between the extracellular and intracellular environments, dramatically disturbing cellular homeostasis[37]. In particular, uncontrolled ion exchanges through the pore dramatically alter the intracellular-ion composition, which triggers host defense mechanisms to repair the inflicted damage and recover cell homeostasis[38]. However, if the damage is too extensive, programmed cell death pathways are engaged.

LLO pores have been shown to induce a plethora of cellular responses, such as control of autophagy upon vacuolar escape[39,40] (Figure 4A), regulation of NOX2 NADPH oxidase activity[41] (Figure 4A), specific histone modifications[42] (Figure 4B), mitochondrial fragmentation[43] (Figure 4B), inflammasome activation[21] (Figure 4B), control of sumoylation machinery[44,45] (Figure 4B) and modulation protein levels[46] (Figure 4B).

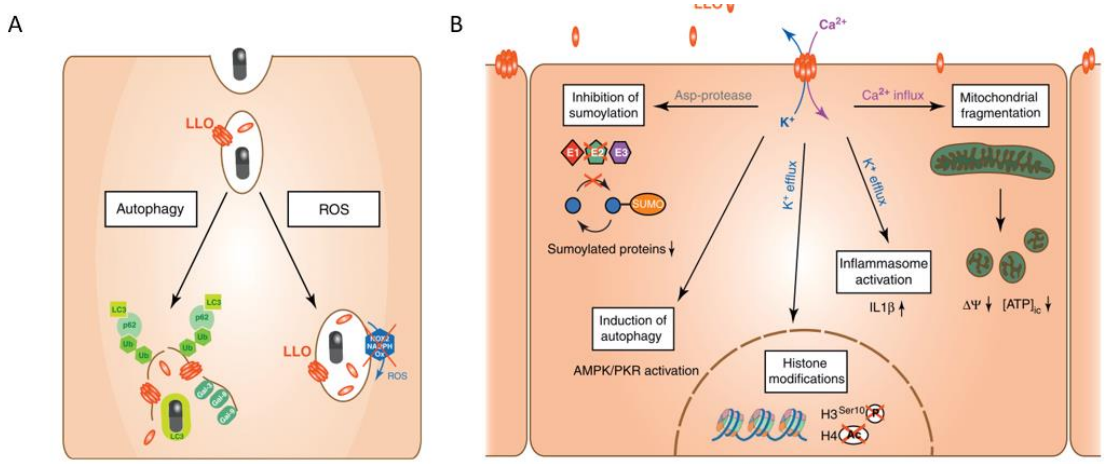

Figure 4. Functions of LLO acting from the extracellular milieu**.** (A) Roles of intracellular LLO during infection. Upon *Lm* internalization LLO plays a key role in the disruption of the vacuole to release the bacteria into the cytoplasm. LLO is also important to avoid autophagy via the expression of *Lm* surface proteins ActA or InlK[39,47]. Membrane remnants recruit ubiquitin (Ub), the autophagy markers p62 and LC3, and galectins (Gal) to allow bacteria escape from vacuole. In parallel, LLO inhibits the NADPH oxidase by preventing its localization to phagosomes thus suppressing reactive oxygen species (ROS) and avoiding bacteria being killed during the respiratory burst. (B) Host cell responses to extracellular LLO. The involved mechanisms and downstream effects are indicated as far as they have been characterized. Although all of these effects require pore formation, ion flux through the pore has been shown to play a role only in the induction of specific histone modifications, mitochondrial fragmentation, and inflammasome activation. Abbreviations: AMPK, AMP-activated protein kinase; PKR, protein kinase receptor; SUMO, small ubiquitin-like modifier. Adapted from Hamon and Cossart, 2012[21].

HeLa cells intoxicated with recombinant LLO caused mitochondria fragmentation in a process that is dependent on calcium influx, but independent from potassium efflux[48]. In addition, mitochondria fragmentation only occurs when LLO acts from the extracellular milieu[49]. In turn, LLO-driven histone modifications[42], inflammasome activation[21] and dysregulation of the sumoylation machinery[44,45] are dependent on potassium efflux (Figure 4 B). The decrease of intracellular potassium concentration acts as a signal that leads to dephosphorylation of H3[26]. Upon this histone modification the transcriptional profile of several genes is modified, importantly several immunity genes are downregulated possibly promoting bacterial survival[42]. Indeed, there is a direct correlation between dephosphorylation of H3 and gene silencing, suggesting a mechanism by which LLO primes the host cell before bacterial invasion[42]. LLO also affects the SUMOylation machinery of the host. SUMOylation is an essential post-translational modification involved in a lot of cellular functions, such as transcription regulation, maintenance of genome integrity, intracellular transport, or stress responses[50]. LLO alters the SUMOylation level of key host proteins and interferes with their activity promoting bacterial replication and dissemination within the host[45]. Moreover, LLO alters the host cell proteome by specifically decreasing the abundance of 149 proteins[46]. This toxin-induced proteome remodeling involves only post-transcriptional regulations with no modification in the transcription levels of the corresponding genes[46].

During infection, most cells are exposed to low concentration of toxins, which would not necessarily lead to cell death[37]. The ability of cells to survive and restore PM integrity following damage caused by PFTs, and the rate with which this occurs depends on cell types, toxin identity and concentration[1]. In this dissertation we will assess repair and pore elimination mechanisms deployed by epithelial cells in response to sub-lytic concentrations of LLO.

1.3 Plasma membrane damage response

The plasma membrane (PM) is the physical barrier that separates the intracellular and extracellular environments ensuring cell homeostasis[51]. As it is the first protective barrier of cells, integrity of the PM is therefore essential for the survival and sustenance of the living cell[52]. PM injury is a severe cellular threat and induces multiple responses, depending on the nature of the damage and the cell type involved[37,51].

The formation of PM pores by bacterial PFTs results in the breaching of the cellular integrity and loss of the barrier function of the target cell membrane, which favors bacterial infection and the successful establishment of the pathogen within its host[52]. PM disruption profoundly alters the intracellular-ion composition, as influx of calcium and efflux of potassium occur in an uncontrolled way through the wound. Such ion imbalance has long been recognized as the primary trigger for cell responses to PM damage[1,53,54]. In particular, the influx of extracellular calcium into the cytosol appears essential to determine the cell fate following PM disruption, either promoting survival or triggering cell death[55]. In particular, the calcium influx induces a cascade of events including the recruitment of membrane repair proteins to the site of the damage to close the membrane pore in a matter of seconds[56,57] (Figures 5 and 6). However, when the PM damage is too extensive, the raise of intracellular calcium concentration is massive and leads to the activation of programmed cell death mechanisms. In a similar way, the efflux of potassium to the extracellular medium and the consequent decrease in intracellular potassium concentration promotes stress-activated pathways that can protect against PFT activity. The drop in cytosolic potassium levels alters the cellular metabolic state, triggers innate immune signaling and can cause pro-inflammatory cell death[58].

The flux of ions depends on the dimension of the PM wound which, in the case of toxin-induced pores, varies greatly according to the structure and size of the pore, receptors involved and stoichiometry, which are all properties defined by the type of the toxin[1,58]. It was demonstrated that the full recovery of PM integrity depends not only on the size and the number of the pores but also on the nature of the wound[59]. While the repair of a mechanical rupture requires addition of lipid components of the PM, a proteinaceous pore inserted in the membrane such it is the case for PFTs, needs to be removed[1]. Counter intuitively, CDCs-induced large PM pores are rapidly repaired (~min), while small toxin pores appear to take longer to be repaired (~h)[56]. This has been mainly attributed to the lower calcium permeability of small pores, and the consequent defect to efficiently trigger calcium-dependent repair mechanisms[37].

At high concentrations, PFTs cause extensive deleterious damage which culminates in cell death, however, at sub-lytic concentrations they trigger repair responses that support cell adaptation and full recovery from the PM damage[60,61]. In mammalian cells the membrane

resealing after disruption generally occurs within 10-30 seconds[62]. Several molecular mechanisms have been proposed to cooperate during PM repair upon PFTs attack and determine the fate of intoxicated cells[37]. In particular, pore clogging, PM blebbing and shedding of vesicles, lysosomal exocytosis and endocytosis may work independently or cooperate to restore PM integrity. Below, I describe in detail each of these mechanisms.

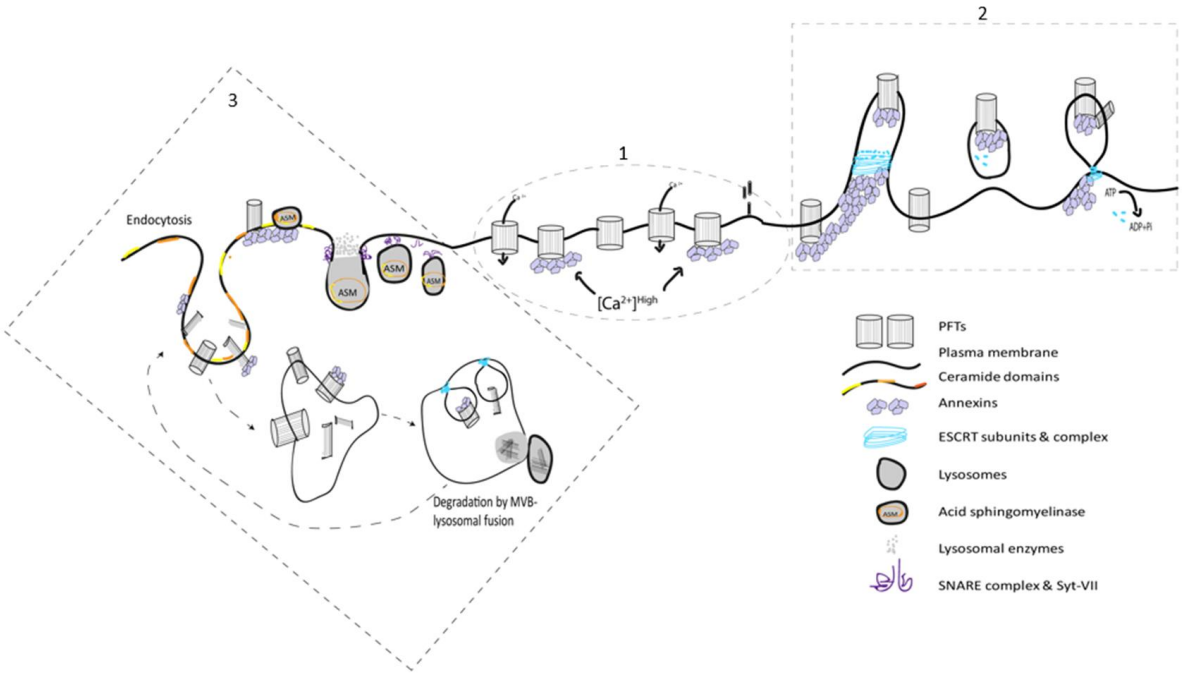

Figure 5. Proposed overview model representing calcium-dependent PM repair mechanisms that protect host cells against PFTs. (1) Upon pore formation there is an influx of extracellular calcium that triggers several mechanisms of PM repair. This increase in calcium leads to the recruitment of specific calcium-sensitive proteins (such as annexins) to the site of the pore. Such proteins form aggregates and assemble in 3D structures that clog the pore avoiding further calcium influx. (2) Mechanisms aiming to eliminate the pore consist in the detachment of PM from the cytoskeleton forming a transient bleb that can be retreated when the membrane is repaired or can be shed through microvesicles that are released to the extracellular medium. (3) Also, lysosomes are recruited to the PM and fuse with it releasing their enzymatic content to the extracellular environment. The hydrolytic enzymes, namely Acid sphingomyelinase (ASM) alters membrane phospholipids from the extracellular environment and consequently induces different PM curvatures which facilitate the endocytosis of the pore and its intracellular degradation.

1.3.1 Pore clogging

PM repair by pore clogging mechanism is particularly important in the sealing of lipid-based wounds such as those created by mechanical or laser-induced damage, however it is also important in the initial response to PFTs-induced damage[63]. Pore clogging involves the

recruitment and accumulation of calcium-responding proteins around the lesion. It is proposed that recruited proteins assemble in a specific 3D array structure forming a barrier that block the wound preventing the loss of cytoplasmic content to the extracellular environment and the excessive calcium influx, and isolating the PM damaged site[53] (Figure 6).

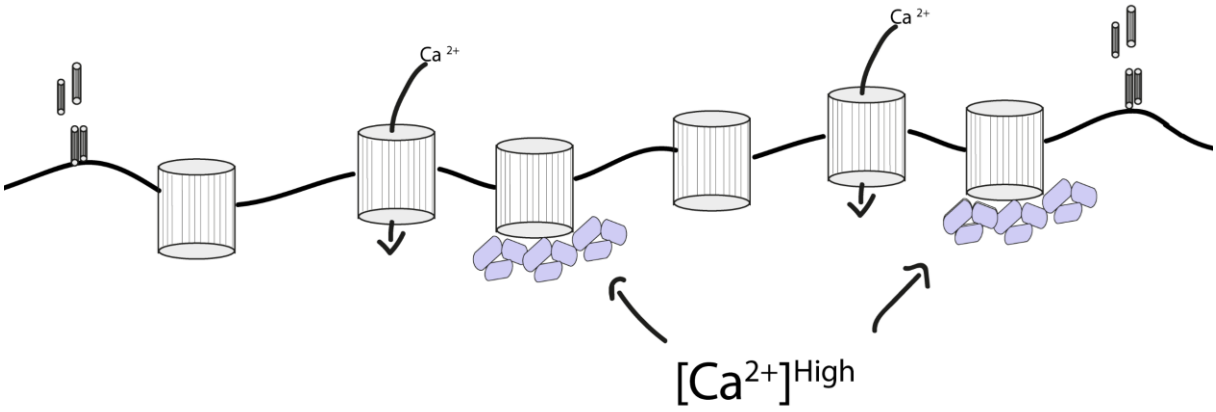

Figure 6. Schematic representation of the pore clogging mechanism. Upon PM pore formation, calcium massively enters in the cell and its intracellular concentration increases. Calcium-sensitive cytoplasmic proteins such as annexins are activated and sequentially recruited to the site of the damage accordingly to their calcium responsiveness. The most sensitive proteins will be activated following a small increase in intracellular calcium concentration and therefore they will be the first to be recruited to the PM. Activated annexins assemble in a 3D structure close to the PM and clog the pore.

Despite to limit the loss of cytoplasmic content and the rise of intracellular calcium to toxic levels, is a critical event during repair of toxin-induced damage, toxin pores do not spontaneously seal and must be actively removed[37]. Thus, in the context of toxin-induced pores, pore clogging might not be sufficient for effective repair and requires the cooperation of other mechanisms (see below).

Among the large variety of proteins described to be involved in pore clogging mechanism, proteins belonging to the annexin family appear to be the main regulators of the process[63]. Annexins (1 to 11 and 13) are cytosolic calcium sensors capable of aggregating, binding phospholipids and promoting membrane fusion in a calcium-regulated manner[64,65]. In response to calcium influx, annexins are activated and sequentially and reversibly translocate to the PM (Figure 6) according to their different calcium sensitivities[66]. Annexins were shown to have protective roles against mechanical or laser-induced PM damage and in PM damage-related disorders[65]. In addition, several annexins were shown to be rapidly recruited to PM lesions in cells damaged by different PFTs[60], however, their role in clogging protein pores and

protecting cells during PFT intoxication remains to be clearly demonstrated. Besides annexins, PM repair likely involves other proteins partners, such dysferlin[67] and other repair components.

1.3.2 Plasma membrane blebbing and shedding of vesicles

PM blebbing and shedding of microvesicles are important PM repair mechanisms protecting the cell from detergent- or mechanically- induced wounds and against intoxication with PFTs (Figure 7).

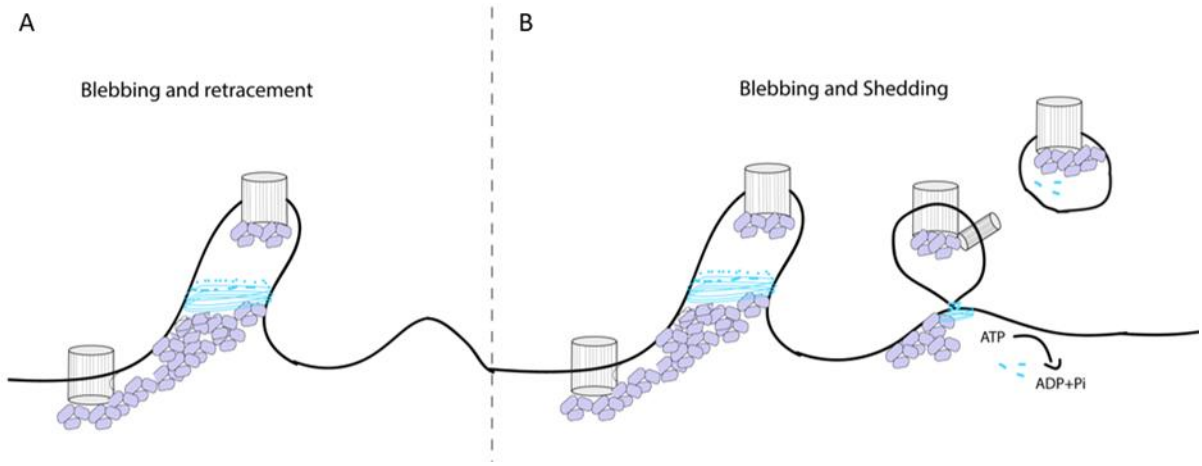

Figure 7. Blebbing and shedding of microvesicles. The increase of intracellular calcium leads to the detachment of the PM from the host cell cytoskeleton, allowing the formation of transient blebs. If the damage is limited the cell can repair the damage, the PM bleb retracts back to the cell body and the PM interconnection with the cell cytoskeleton is restored. Under certain circumstances, which are not fully understood, the bleb does not retract being shed from the cell surface and released to the extracellular environment.

Blebs are cell PM protrusions[68]. Blebbing is a general cellular response mechanism to PM injury, which is also well described in other processes such as cytokinesis, cell migration, and apoptosis[68,69]. PM bleb formation occurs in response to calcium influx and rely on the actomyosin contraction and on the disruption of PM–cytoskeleton interactions, which reduces the PM tension and allows its expansion. PM blebbing at the sites of damage together with the recruitment and assembly of 3D annexin arrays, are proposed to cooperate to PM repair by isolating the damaged PM fraction and limiting the massive calcium influx within the target cell cytoplasm (Figure 7). Following damage repair and the consequent decrease of intracellular calcium signaling the actomyosin cytoskeleton re-establishes the interactions with the PM and the bleb retracts back towards the cell body [68,70].

Alternatively to bleb retraction, PM blebbing enables the shedding of microvesicles, which is also regarded as a major PM repair mechanism. Besides protecting from detergent- and mechanically-induced wounds, shedding of microvesicles are effective against intoxication by PFTs creating either small or large pores[33,55,71,72]. Several lines of evidence suggest that the elimination of PFTs from the PM is achieved by the release of PM vesicles that contain the pore (Figure 7). Indeed, shedding of vesicles has been described in response to several PFTs and was demonstrated as a key mechanism in the repair of PFTs pores[73,74]. It is though that repair through shedding of microvesicles requires the cooperation of annexins which rapidly confine and clog the pore limiting excessive damage. Then the release of the pore to the extracellular medium would occur with minimal injuring consequences, allowing the cell to return to its normal state of function. Microvesicle shedding thus allows early elimination of toxin pores allowing the survival of damaged cells[73].

PM blebbing and shedding might constitute an intrinsic protection mechanism which is further improved by toxin oligomerization, pore formation, and calcium entry[71,72]. The release of large PM structures along with the shedding of smaller blebs would allow not only the removal of PFT pores[75] and the disposal of irreversibly damaged organelles[76], but also the release cytoplasmic inflammatory signals[75].

In summary, PM blebbing occurs at wound sites, and includes passive PM shedding, active vesicle budding, and release of vesicular structures enriched in endosomal sorting complex required for transport (ESCRT) proteins, annexins, PFT pores, and other molecules[70,72,73,75].

1.3.3 Lysosomal exocytosis and endocytosis

Exocytosis of cortical lysosomes was proposed to patch PM wounds[77,78] thus participating in PM repair. This mechanism is particularly important in the process of spontaneous sealing of lipid lesions, such as laser- or mechanically-induced PM wounds[79]. It is though that the fusion of intracellular vesicles, such as lysosomes, with PM at sites of damage promote a drop in PM tension, a key event in spontaneous repair. In addition lysosomes can provide membrane material to repair the wound[73]. The increase in intracellular calcium concentration induces a cascade of events including recruitment of membrane repair proteins to the site of injury (as described above) and of intracellular vesicles[57], mainly lysosomes[80,81], which fuse with PM delivering their content into the extracellular milieu (Figure 8).

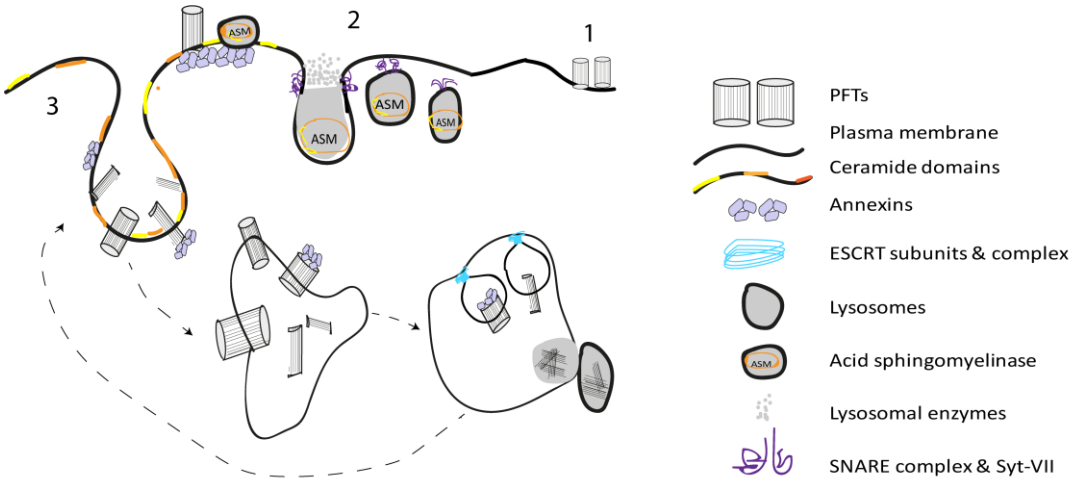

Figure 8. Lysosomal exocytosis and PM endocytosis. (1) The binding of soluble monomers allows toxin oligomerization and pore formation. (2) Calcium influx permits the recruitment of lysosomes to the PM. Interactions and docking of the lysosomes with the PM depend on the assembly of SNARE complexes wich are driven by the calcium sensor Synaptotagmin VII (Syt-VII). Upon docking, lysosomes fuse with the PM and deliver their content to the extracellular milieu. Among others lysosomal acid sphingomyelinase (ASM) is released. (3) ASM hydrolyses PM sphingomyelin, producing ceramide domains, which facilitate membrane invagination and endocytosis. Ceramide domains may also contribute to annexin recruitment. PFTs traffic to MVBs through ESCRT-dependent sorting and are degraded via MVB–lysosomal fusion.

Small GTPases (Rab3, Rab10, and Arl8b) and the actin motor protein non-muscle myosin IIA (NMIIA) control the cortical localization of lysosomes that is required for PM repair[82]. Briefly, the rise in cytosolic calcium activates Rab3 and promotes actin remodeling contributing to recruitment, binding, docking, and fusion of cortical lysosomes with the PM[56]. The binding and docking of lysosomes with the inner leaflet of the cell PM involves calcium-dependent interactions between the calcium sensors such as synaptotagmin VII, dysferlin, and lysosomal and PM SNARES[81,83–85]. Interestingly, lysosome exocytosis upon PM damage, is reminiscent to the secretion of granules by cytotoxic lymphocytes or professional secretory cells. Indeed, the fusion of cortical lysosomes with PM and the consequent extracellular delivery of lysosomal enzymes are not only important for the repair of PM but have also been proposed as an autonomous defense mechanism against pathogens that damage the PM of the host cell[85].

Among the lysosomal enzymes delivered to the extracellular milieu, the acid sphingomyelinase hydrolyses PM sphingomyelin, producing ceramide domains, which facilitate membrane invagination and endocytosis of PFTs' pores and/or incomplete pore

structures. Ceramide domains may also contribute to annexin recruitment. Despite the exact role of endocytosis in pore removal is still under debate, it has been increasingly clear that the endocytic proteins have important functions in efficient repair and contribute to the survival of cells upon intoxication. Endocytic components such as caveolin-1 and GRAF1 were recently demonstrated to play a role during PM repair of PFT pores by acting on the remodel and regeneration of the normal composition of the PM following repair[86]. Based on ultra-structural studies, a recent report proposed a model in which the active pores induced by PFT are removed by shedding microvesicles, while endocytosis restores PM homeostasis, removing inactive PFT monomers and vesicles that were not eliminated when the repair is complete[86].

Besides being critical to promote endocytosis at the site of damage, lysosome exocytosis may be linked to PM shedding. In glial cells, secretion of ASM promotes PM shedding of phosphatidylserine (PS)-rich vesicles downstream P2X7R activation. This process is dependent on the activation of p38[87], and per se may explain the removal of small PFTs pores, which do not trigger a massive Ca-mediated repair. Additionally, the release of vesicles upon lysosomal exocytosis may promote the secretion of cytokines downstream the activation of p38[87].

In summary, current data points that clogging of the pore, PM blebbing, shedding of vesicles, and lysosomal exocytosis and endocytosis are interconnected mechanisms that cooperate to respond to PFTs and to promote cell survival.

1.4 Context of this master thesis: main objective

The group of Cell Biology of Bacterial Infections (CBBI) focus its research on interactions between host and pathogen. During infection, the pathogen exploits the cellular functions to hide from immune defense and establish within the host. In turn, the host deploys resistance mechanisms to repair damage and survive to infection. The main goal of CBBI is to uncover cell biology processes and signaling pathways that are involved in the response of the host to the pathogen. In particular, CBBI members are interested on cytoskeleton remodelling induced by pathogens[37].

For several years, CCBI assessed host cytoskeleton alterations induced by *Listeria monocytogenes* during its intracellular infection. Researchers found that *Lm* exploits the function of actomyosin[88,89], keratins[90] and tubulin[91] to promote cellular invasion and cell-to-

cell spread during infection of epithelial cells. More recently, they become interested by the mechanisms deployed by the host cells to resist and repair PM damage induced by PFT, which are major virulence factors expressed by several human bacterial pathogens with clinical relevance. Members of CCBI showed that upon PM damage induced by PFTs, human epithelial cells undergo massive actomyosin remodelling[38,92]. PM repair, recovery of cell integrity and host survival to infection are dependent on the assembly of cortical actomyosin structures in the target cell. In addition, they demonstrate the critical role of actomyosin cytoskeleton and endoplasmic reticulum components in the PM repair of pores created by several bacterial PFT[37,38,92].

To identify new mechanisms and novel host factors involved in the response to PFTs by promoting PM repair and host survival, CBBI engaged in several broad approaches among which a gain-of-function global approach that I will detail in the next section. Vav3 emerged as a candidate promoting cell survival in response to lytic concentrations of LLO. The main objective of my project was to validate the role of Vav3 in the host cell response to LLO.

1.5 Gain of function approach to identify novel factors involved in cell survival to PFTs

In a search for new host factors that could contribute to PM repair upon intoxication thus allowing cell survival, the CBBI performed a forward genetic screen based on a gain-of-function approach. This screen was based in the assumption that: if a given protein is important for host cell survival upon PFTs attack, cells that overexpress such protein would be more resistant to intoxication. A similar approach was previously used to systematically identify proteins conferring chemotherapy resistance to cancer cells[93].

A library of mutagenized human cells was generated by random insertion of a transposon (Figure 9). Transposons are mobile genetic elements that insert randomly into the genome by a process named transposition[93].

A major advantage of transposons is the simplicity of their integration mechanism, which allows the incorporation of long DNA sequences, including functional genetic elements such as promoters, transcriptional stops and splicing sequences[94]. This flexibility has allowed development of a variety of powerful mutagenesis schemes.

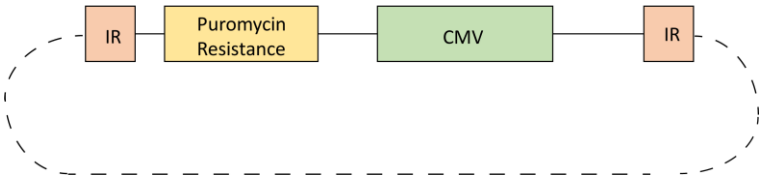

Figure 9. Schematic representation of the transposon used. The cytomegalovirus strong promoter is drawn as CMV, IR represent the invert repeats that are transposon insertion regions in the genome and puromycin resistance represent the cassette of selectable marker. The region between the two IR sequences was inserted randomly in the genome of mammalian cells.

The transposon used (Figure 9) in this screen harbour a gene conferring resistance to puromycin and enhancer and promoter sequences of the cytomegalovirus (CMV). This CMV promoter is a strong promoter commonly used to overexpress proteins in mammalian cells. These genetic determinants (CMV enhancer and promoter sequences) allow the overexpression of the genome sequence downstream the insertion site.

HeLa cells were transfected with the plasmid harbouring the transposon (Figure 9) described above and cells containing the transposon inserted in their genome were selected by adding puromycin to the medium (Figure 10).

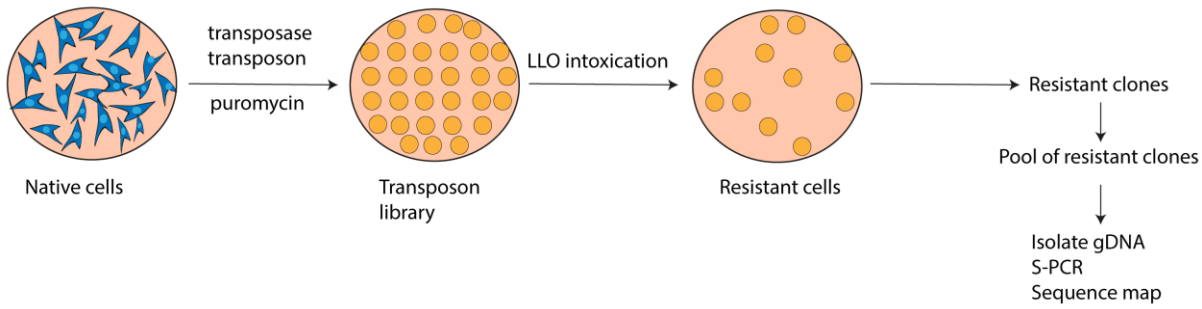

Figure 10. Mutagenesis and screen flow chart.

The library of transposon-inserted mutants was then challenged with lethal doses of LLO. Most of the cells died from intoxication. However resistant cells were selected, amplified and sequenced to identify the transposon insertion site. Accordingly with our initial assumption, the sequences located downstream of the transposon insertion site were overexpressed and may thus confer a survival advantage to LLO intoxication.

One of the candidates to promote cell survival upon LLO intoxication identified in this screen is the coding sequence for the protein Vav3, a regulator of small GTPases and actin

cytoskeletal rearrangements. This master thesis project thus proposes to validate the potential role of Va3 in the host's response to LLO attack.

1.6 Small GTPases: their functions and their regulators

The Ras homologous (Rho) family of small GTPases constitute one of the five main arms of the Ras superfamily and includes 20 members in humans[95]. The Rho GTPases are highly conserved proteins found in all eukaryotic cells[96]. They are a class of small molecules mainly known for their key roles in the regulation the actin organization, cell motility, growth and survival[96–100], among many others. Furthermore, they were described to participate in cell-specific processes such as immune response[101], angiogenesis[101] and neurogenesis[102].

Small GTPases exhibit high-affinity binding for GDP and GTP and, in cells, they alternate between GDP-bound and GTP-bound state acting as binary switches that are active if GTP-bound and inactive in GDP-bound state (Figure 11). Upon GTP binding, GTPases undergo conformational changes that promote the interaction with effector proteins triggering downstream signalling pathways and thus generating appropriate cellular responses[103]. GTPases possess low intrinsic GTP hydrolysis and GDP/GTP exchange activities. GDP/GTP cycling is controlled by two main classes of regulatory protein. Guanine-nucleotide-exchange factors (GEFs) promote formation of the active, GTP-bound form whereas GTPase-activating proteins (GAPs) accelerate the intrinsic GTPase activity to promote formation of the inactive GDP-bound form (Figure 11)[104]. Through direct interaction GEFs and GAPs have the capacity to regulate spatiotemporal activity of GTPases[105].

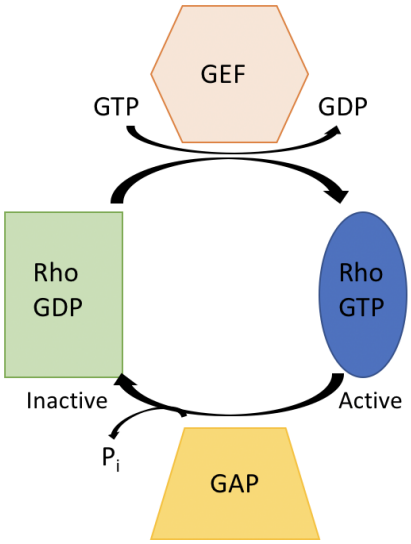

Figure 11. Rho GTPase regulation. GTPase-activating proteins (GAPs) increase the low intrinsic GTP hydrolysis activity converting active GTPases in their inactive GDP-bound form. In turn, guanine nucleotide exchange factors (GEFs) promote the binding of GTP, inducing a conformational modification and leading to the formation of the active GTP-bound form. Several GTPases also combine their GDP/GTP switch with a cytosol/membrane alternation regulated by GDIs or GDI-like proteins[106].

1.6.1 Vav proteins are guanine nucleotide exchange factors

Vav proteins an evolutionary conserved from nematodes to mammals[107] and play major roles in cellular signalling. In vertebrates three Vav family members are described (Vav1, Vav2, and Vav3), while in invertebrates single representatives are reported (C. elegans Vav and D. melanogaster Vav)[108]. Vav proteins are missing in unicellular organisms and plants[109].

In mammals, Vav1 is expressed predominantly in hematopoietic-derived cells[110] whereas Vav2 and Vav3 are ubiquitously expressed[111]. Vav family members act as GEFs towards small GTPases Rho/Rac, being able to activate Rac as well as RhoA and RhoG[112]. In vitro, Vav proteins were shown to promote the activation of Rac subfamily GTPases (Rac1, RhoG) and, to a lower extent, of Rho subfamily (RhoA)[113]. Consistent with their activity as GEFs, Vav proteins participate in several cellular processes that require cytoskeletal organization, such as the formation of immunological synapse, phagocytosis, integrin-mediated signalling, wound healing and migration, among others[107].

The importance of the Vav family-dependent pathways *in vivo* was demonstrated by the analysis of the phenotypes of mutations in model organisms. In the case of Vav2- and Vav3-deficient mice, defects were also observed outside the hematopoietic system. Those

include dysfunctions in axon guidance, angiogenesis, bone remodeling, cerebellar development, blood pressure regulation, and metabolic disease[109].

The GEF activity of Vav family members is regulated by tyrosine phosphorylation[111]. In response to an extracellular stimulus inactive Vav proteins interact with the activated receptor tyrosine kinases and become phosphorylated in specific tyrosine residues[114]. The tyrosine phosphorylation of Vav proteins induces conformational changes which enable their interaction with small GTPases and their corresponding activation[115].

1.6.2 Vav domains and their functions

Vav proteins display several structural motifs that allow them to function as signal traducing proteins[115,116] (Figure 12). They include eight different structural domains: a conserved N-terminal calponin homology domain (CH) involved in calcium mobilization and transforming activity, an acidic domain (AC) containing three regulatory tyrosine residues, a catalytic Dbl homology (DH) region involved in the guanosine nucleotide exchange activity, a pleckstrin homology (PH) domain typical of members of Rho/Rac GEFs binding to PIP3 and enabling its recruitment to the inner leaflet of the PM, a zinc finger (ZF) domain and two Src-homology 3 (SH3) regions, which may interact with proteins containing proline-rich sequences, flanking a single Scr-homology 2 (SH2) domain that interacts with proteins containing phosphorylated tyrosines (Figure 12)[116].

Figure 12. Schematic representation of different domains of Vav3 proteins. All Vav family members can be divided in eight different structural domains: a calponin-homology (CH) region, an acidic (AC) domain, a Dbl-homology region (DH), a plesckstrin-homology (PH) domain, a zinc finger (ZF) region, two SH3 domains and a SH2 region[115].

It was proposed that each structural domain has multifunctional roles, participating in intramolecular regulatory actions, proteins-protein interactions, and/or effector roles[117]. The CH, AC and most C-terminal SH3 regions participate in phosphorylation-dependent intramolecular interactions that regulate the function of Vav proteins and, at the same time, establish physical interactions with other proteins[109]. Also, Vav family is the only group of

signal transduction proteins known to date combining a DH-PH cassette with ZF and SH2 regions[108].

In particular, DH domain is the GEF activity domain that interacts directly with Rho GTPases and plays a catalytic role for Vav family members[118]. For that, DH domain play a catalytic role in the switch between GDP (inactive state) to GTP (active state)[119].

The PH region have a role in the translocation of proteins to the plasma membrane[116]. Functionally, PH domains are known to mediate membrane association via binding to PIP2 and/or PIP3. Studies shows that PH domains mediate membrane association via high affinity binding to membrane phospholipids[120].

The Vav family SH2 domains are crucial for the activation of Vav proteins during signal transduction because they allow the interaction of the inactive Vav proteins with a broad spectrum of activated transmembrane and cytoplasmic tyrosine kinases. These proteins interact with tyrosine phosphorylation sites and/or indirectly with activated tyrosine kinases by binding to adapter proteins that contain SH2 and/or SH3-binding motifs, Vav proteins can interact directly with several tyrosine kinases[121]. Thus, Vav become tyrosine phosphorylated in its SH3 or SH2 domains, during the activation of signaling cascades initiated by receptors tyrosine kinases located at the cell surface[118,119].

Vav proteins demonstrated crucial signaling roles in a large variety of organisms and cell types, including those belonging to the immune, nervous, and cardiovascular systems. These proteins are thus critical in physiological processes such as adhesion, migration and development but they were also associated with pathological conditions such as cancer and immune-related disfunctions[118]. The activity of the Rho family GTPases greatly influences the actin cytoskeleton rearrangements. As other regulators of the Rho GTPases, by modulating the activities of Rho and Rac, Vav proteins mediate they regulate the organization of the cytoskeleton and participated in a several cytoskeletal-associated cellular processes such as cell division, growth, adhesion and locomotion[107].

This dissertation focus on the possible role of Vav3 in the host cell response to the attack by the bacterial toxin LLO. Vav3 codifying region was previously identified as a hit in a gain-of-function screen aiming at identifying genes whose overexpression benefits cell survival in response to PFTs. This suggest that Vav3 may participate in the repair of PM damage induced by a PFT, a process that is highly dependent on actomyosin cytoskeleton remodeling. Supporting this hypothesis, Vav3 was shown to participate in signal transduction

processes and in the activation of several members of the Rho family like RhoA, RhoG and Rac1[112]. In addition, it was recently found that Vav3-induced cytoskeletal dynamics contribute to heterotypic properties of endothelial barriers[122].

2. Materials and Methods

2.1 Cell lines and culture media

Human epithelial cell line HeLa (ATCC CCL2) was propagated in Dulbecco's Modified Eagle's Medium (DMEM) with glucose and L-glutamine (Lonza, Switzerland), supplemented with 10 % fetal bovine serum (FBS; Biowest, France). Cells were maintained at 37 ˚C in a 5 % CO_2 atmosphere. Incubations with purified LLO and washes were carried out in Hanks' balanced salt solution (HBSS; Lonza, Switzerland).

2.2 Plasmids, antibodies and dyes

The plasmids pC.HA (# 15126) and pC.HA Vav3 (# 14555) were obtained from Addgene and were made available by Dr Joan Brugge[115]. pC.HA Vav3 allows the overexpression of Vav3 in mammalian cells in fusion with a tag HA, which can be detected by an anti-HA antibody. Plasmids encoding Vav3-GFP variants (namely the WT version of the protein, PH mutant W493L, GEF mutant (ISO) and the pIRES-Vav3 plasmid) were kindly offered by Professor Kerry Burnstein[123]. These plasmids allow the overexpression of Vav3 and the green fluorescent protein (GFP) in mammalian cells. GFP can be detected directly detected by fluorescence emission or by an anti-GFP antibody.

For immunofluorescence (IF) microscopy analysis, cells were labelled with a mouse monoclonal anti-HA antibody [16B12] (ab130275, Abcam) diluted 1:200. An anti-mousse Alexa Fluor 488 (Molecular Probes, Invitrogen) secondary antibody was used at a dilution 1:200. Actin was stained with phalloidin coupled to Alexa Fluor 647 (Molecular Probes, Invitrogen) or Alexa Fluor 546 (Molecular Probes, Invitrogen). Nuclei were stained with DAPI, which binds DNA, diluted at 1:1000 (Sigma).

For western blot analysis, membranes were incubated with mouse anti-HA diluted (1:500) [16B12] (ab130275, Abcam), mouse anti-actin (1:20000) (SIGMA); rabbit anti-GFP (1:1000) (homemade antibody). Secondary antibodies were used at 1:2000; anti-mouse or anti-rabbit coupled to HRP (P.A.R.I.S).

2.3 Toxins and intoxications

Recombinant LLO was purified as described [124]. Intoxications were performed in 6-well plates in a total volume of 2 mL of HBSS without phenol red (Lonza) containing the indicated concentrations of LLO for 20 min. After intoxication, cells were washed with PBS 1x and either immediately processed for analysis or allowed to recover in DMEM supplemented with 10 % FBS for the indicated time periods.

2.4 Purification of the plasmids pC.HA and pC.HA Vav3

The plasmids pC.HA and pC.HA Vav3 obtained from Addgene were delivered in *Escherichia coli* stabs in solid medium. *E. coli* strains harboring the plasmids were isolated in Lysogeny Broth (LB) agar plates supplemented with 100 µg/mL ampicillin. The plates were incubated overnight at 37 ˚C. Grown colonies were then inoculated in liquid LB medium containing 100 µg/mL ampicillin and incubated overnight at 37 ˚C with agitation. The plasmids were purified from saturated culture using QIAGEN Plasmid Midi Kit (QIAGEN), following the manufacturer's protocol for high copy number plasmids. Briefly, bacterial cells were recovered by centrifugation and lysed in a specific buffer containing detergent. The clarified lysate was applied into a column that retains the plasmid, washed and the DNA was eluted. Finally, the plasmids were precipitated, washed and resuspended in ultra-pure water. The concentration and the quality of the purified plasmids were evaluated using NanoDrop. pC.HA was obtained at a concentration of 270.5 ng/µL and pC.HA Vav3 at 2158 ng/µL.

2.5 Digestion of plasmid pC.HA and pC.HA Vav3

By definition, 1 unit of restriction enzyme (U) will completely digest 1 µg of substrate DNA in a 50 µl reaction in 60 minutes. Plasmid pC.HA (1ug) was digested for 1 h at 37 ˚C with 20 U of restriction enzyme BamHI (NEB), in 1x digestion buffer (CutSmart, NEB) and a total reaction volume of 50 µL.

Volume of pC.HA to have 1 µg of plasmid:

$$\mathrm{c} = \frac{m}{v} \leftrightarrow \mathrm{v} = \frac{1\ \mu g}{270.5 \times 10^{-3} \mu g/\mu L} \leftrightarrow v = 3.70\ \mu L$$

Same quantity of plasmid pC.HA Vav3 (1 µg) was digested 1 h at 37 ˚C with 20 U of BamHI (NEB) and 10 U of XbaI (Fermentas) in 1x digestion buffer (CutSmart, NEB) and a total reaction volume of 50 µL.

Volume of pC.HA Vav3 to have 1 µg of plasmid:

$$\mathrm{c} = \frac{m}{v} \leftrightarrow \mathrm{v} = \frac{1\ \mu g}{2158 \times 10^{-3} \mu g/\mu L} \leftrightarrow v = 0.46\ \mu L$$

Digestions were verified by electrophoresis in a 1 % agarose gel in TAE buffer. To stain DNA, the gel was supplemented with GreenSafe Premium (nzytech), that binds DNA and emits green fluorescence. To determine the size of the DNA bands, DNA standard ladder was used as molecular weight marker (HyperLadder 1 Kb, Bioline). The samples (27.5 µL from the 50 µL) were mixed with loading buffer (Biolabs), loaded in the gel and submitted to electrophoresis for 25 min at 100 V.

2.6 Transfection of HeLa cells

Transfections of HeLa cells were performed in 6-well plates using Jetprime (Polyplus), following the manufacturer instructions. Briefly, 6×10^5 cells were mixed with 2 µg of plasmid DNA, 200 µL of transfection buffer and 4 µL of transfection reagent, in a total volume of 2 mL of medium and plated in a single well. Cells were incubated for 3.5 h at 37 ˚C in a 5 % CO_2 atmosphere, then carefully washed 3 times with DMEM+10 % FBS and incubated at 37 ˚C in a 5 % CO_2 atmosphere in fresh complete medium. Assays were performed 24 h post-transfection.

2.7 Western Blot Analysis

Protein extracts were resolved by SDS-PAGE in a 10 % (v/v) polyacrylamide gel. Approximately 1×10^6 cells were directly lysed in 4x Laemmli buffer containing 5% ß-mercaptoethanol and the samples were denatured at 95 ˚C for 10 mins. Total protein extracts from approximatively 3×10^5 cells were separated according to their molecular weight by SDS-PAGE and transferred (Trans-Blot Turbo Transfer System; Bio-Rad Laboratories) onto a nitrocellulose membrane, according to the manufacturer's guidelines, during 1 h at 100 V. Nitrocellulose membranes were staining with Ponceau S dye (Sigma) and blocked with a 5 %

skimmed milk diluted in PBS supplemented with 0.05 % tween. Then, the membranes were incubated with agitation overnight at 4 ˚C with mouse anti-HA antibody diluted in 2.5 % skimmed milk in PBS supplemented with 0.1 % tween. After three washes with PBS with tween 0.2 % for 10 min at room temperature, membranes were probed with anti-mouse HRP-conjugated secondary antibodies diluted in 2.5 % skimmed milk diluted in PBS with 0.1 % tween for 1 h at room temperature. Upon membrane wash with PBS with tween 0.2 % for 10 min, three times, immunolabeled proteins were detected by chemiluminescence using PierceTM Western Blotting Substract kit (Thermo Fisher Scientific) and the signal was recorded by ChemiDoc XRS + equipment (Bio-Rad Laboratories).

2.8 Flow Cytometry Analysis of LLO intoxicated HeLa cells

For flow cytometry, 6×10^5 HeLa cells/well were seeded and transfected in 6-well plates 24 h before intoxication as indicated below, trypsinized using TrypLE Express (Gibco) and resuspended in phosphate buffer solution (PBS) 1x containing 2 % FBS. Propidium Iodide (PI), which binds double-stranded DNA becoming fluorescent was added to the cells at 5 µg/mL. PI is excluded from cells having intact PM and was thus used to discriminate permeabilized from non-permeabilized cells. At least 20000 cells were analyzed for each sample. Cell were analyzed in a BD Accuri C6 (BD Biosciences, San Jose, CA, USA), and the data obtained were analyzed using FlowJo software (version 10.0.8, TreeStar, Ashland, OR, USA).

2.9 Immunofluorescence Microscopy

Cells were fixed in 4 % paraformaldehyde (20 min at 4 ˚C) and subsequently permeabilized with 0.1 % Triton X-100 for 5 min. Coverslips were incubated for 1 h with primary antibodies diluted in PBS containing 0.1 % BSA, washed in PBS and incubated for 45 min with the corresponding secondary antibodies, DAPI and Phalloidin-Alea 647 diluted in PBS containing 0.1 % BSA. Coverslips were washed in PBS and finally in distilled water before mounting onto microscope slides with Aqua-Poly/Mount (Polysciences, Warrington, PA, USA). Images were collected using epifluorescent Olympus BX53 microscope equipped with a 60 × 0.75 NA objective or Leica SP5II confocal laser-scanning microscope equipped with 63 × 1.4 NA objective and processed using FIJI[125].

IF quantifications were performed in at least 200 cells per sample and in at least three independent experiments. For transfection rate calculation, cells were scored positive when displaying green fluorescence. DAPI nuclear staining was used to quantify the number of total cells per field.

2.10 Generation of Vav3 variants fused with green fluorescent protein (GFP)

The constructs with Vav3-pIREs, Vav3-WT, Vav3-ISO and Vav3-W493L kindly offered by Professor L. Burnstein were cloned in a pIRES vector[126]. *E. coli* strains harboring the plasmids were isolated in petri dishes containing LB agar supplemented with 30 µg/mL kanamycin. The plates were incubated overnight at 37 ˚C. Several colonies grown were inoculated in liquid LB medium containing 30 µg/mL kanamycin and incubated overnight at 37 ˚C with agitation. Plasmids were purified from a saturated liquid cultures using QIAGEN Plasmid Mini Kit (QIAGEN) as indicated by the manufacturer. The concentration and the quality of the purified plasmids was evaluated under NanoDrop.

A total of 1 µg of purified Vav3-WT, Vav3-ISO, Vav3-W493L and Vav3-pIREs was individually digested with 10 U of EcoRI (Roche) and 20 U of SalI (NEB), in 1x digestion buffer (CutSmart, NEB) during 1 h at 37 ˚C.

In parallel, the sequence the constructs Vav3-WT, Vav3-ISO and Vav3-W493L were confirmed by DNA sequencing analysis with the primers 1 and 2, listed on Table 2. The sequence of the different construct was amplified by Polymerase Chain Reaction (PCR) using the gene-specific primers 3 and 4, listed on Table 2. PCR fragments were purified and digested with 10 U EcoRI (Roche) and 20 U SalI (NEB) in 1x digestion buffer (CutSmart, NEB) during 1 h at 37 ˚C. The digested fragments were then colligated in the multiple cloning site (MCS) of the plasmid pEGFP-N2, previous digested with the same restriction enzymes; to generate Vav3 fusions with GFP sequence encoded in pEGFP-N2.

Positive clones were verified by PCR using primers two pairs (6-1 and 7-2) and by DNA sequencing analysis.

Table 2. Sequence of the oligonucleotides used to construct the different Vav3-GFP variants. Capital letters in primer sequences show the restriction sites

	Primers (sigmaaldrich®)	Sequence (5' -3')	Localization
1	vav-primer 1- seq rv	aaacgtctcacaacaggcc	Vav3
2	vav primer 2- seq fw	aacattcagctggacagagg	Vav3
3	vav3-cloning primer rv	agtGTCGACttcatcctcttccacatatgtg	Vav3 insert
4	vav3-cloning primer fw	gctaccggactcagatctcg	Vav3 insert
5	sequencing primer 3 fw	ctcttcgagacttgcttgtgg	Vav3 insert
6	primer cmv fw	cgcaaatgggcggtaggcgtg	pEGFP-N2
7	primer egfp-n1 rv	gtccagctcgaccaggatg	pEGFP-N2

2.11 RNA Extraction and Quantitative RT-PCR

HeLa cells (3×10^5) were seeded in 6-well 24 h before the intoxication with 0.2 nM LLO for 20 min. Cells were washed 3 times with PBS and incubated for growing time periods in complete medium at 37 ˚C in a 5 % CO_2 atmosphere to allow recovery. Cells were collected at 0, 2, 4 and 6 h of recovery and total RNA was isolated following the phenol-chloroform method as previously described[127]. Briefly, after cell lysis total RNA was purified using the TripleXtractor reagent (Grisp) following the manufacturer's recommendations. RNA purity and integrity were verified by 1 % (w/v) agarose gel electrophoresis and Experion Automated Electrophoresis System (Bio-Rad Laboratories). RNA (1 µg) was reverse-transcribed into cDNA using NZY First-Strand cDNA Synthesis Kit. qPCR was performed using 1 µg of cDNA in a 20 µL reaction volume using the iTaq™ Universal SYBR® Green Supermix (Bio-Rad Laboratories) and qPCR detection system (iQ5, Bio-Rad Laboratories). The following cycling protocol as used: 1 cycle at 95 ˚C (3 min); 40 cycles at 95 ˚C (10 s), 54 ˚C (20 s) and 72 ˚C (20 s). Primer sequences are described in Table 3. The human housekeeping gene hprt1 was used as control and data are normalized to the values of the control.

Table 3. PCR primers

	Primers (sigmaaldrich®)	Sequence (5'-3')
1	qpcr *vav3* fw	aatgatatacgaagttgttgtc
2	qpcr *vav3* rv	gttcaggaatgttgatgaatactg
3	qpcr *hprt1* fw	ggcgtcgtgattagtgatg
4	qpcr *hprt1* rv	caccctttccaaatcctcag

2.12 Statistical Analyses

Statistical analyses were performed with Prism version 8.4.3 (GraphPad Software, La Jolla California USA, www.graphpad.com). Using Two-way ANOVA with multiple comparations analysis was used to compare the means of samples within each condition for dose response and recovery assays and One-way ANOVA with multiple comparations analysis for RNA assays. Mean differences were considered statistically non-significant (ns) when p value was above 0.05. For statistically significant differences: * $p \leq 0.05$; ** $p \leq 0.01$; *** $p \leq 0.001$; **** $p \leq 0.0001$.

3. RESULTS

The gene encoding Vav3 was identified in a gain-of-function screen as possibly involved in the response of the cell to the attack of the PFT LLO, the aim of this project is to evaluate the involvement of Vav3 in cell survival against LLO pore formation. For that, we overexpress Vav3 in cells and evaluate whether Vav3 overexpressing cells are more resistant to PFTs and survive better upon PFT-induced PM damage.

3.1 Verification of pC.HA and pC.HA Vav3 plasmids

To overexpress Vav3 in cells, a plasmid harboring the Vav3 encoding sequence under the control of a strong promoter (pC.HA Vav3), as well as, the corresponding control plasmid (pC.HA, empty plasmid) were obtained from Addgene (www.addgene.org). Before starting the overexpression experiments, we verified the plasmids obtained by different approaches, we: 1) use restriction enzymes to confirm the size of the vector and the size of the insert Vav3 encoding sequence and 2) transfect cells and use their total proteins extracts to evaluate the expression of a protein with the molecular size of Vav3 (98 kDa) that would be detected by an anti-HA antibody.

To confirm the nature of the plasmids we selected restrictions enzymes which would cut the empty plasmid in a single site and release the insert corresponding to the Vav3 sequence. This approach should allow to confirm the size of the empty plasmid (pC.HA) and the size of the insert Vav3 (pC.HA Vav3). Thus, the plasmid pC.HA was digested with BamHI which cuts in a single site at the Multi Cloning Site (MCS, Figure 13A) and should linearize the plasmid. The plasmid pC.HA Vav3 was digested with BamHI and XbaI which are the enzymes used in the original cloning of the insert. pC.HA Vav3 simultaneously digested by BamHI and XbaI should give rise to two fragments (Figure 13B): the vector backbone (5.4 Kb) and the insert corresponding to the Vav3 sequence (2.5 Kb).

As expected, the digestion of pC.HA by BamHI gave rise to a single band in the gel with a molecular weight that is compatible with the described size for this vector (5.4 Kb). The non-digested vector migrates at a slight increased size which relates with the conformation of the circular DNA. The digestion of pC.HA Vav3 with XbaI and BamHI leads to the detection of two bands. One that migrates at the same molecular weight than the pC.HA empty vector, that

corresponds to the vector backbone, and another with a size compatible with the insert Vav3 sequence (2.5 Kb). In agreement with the presence of the insert, the undigested pC.HA Vav3 migrates at a higher size than pC.HA. These data suggested that the plasmids that we got from Addgene were correct.

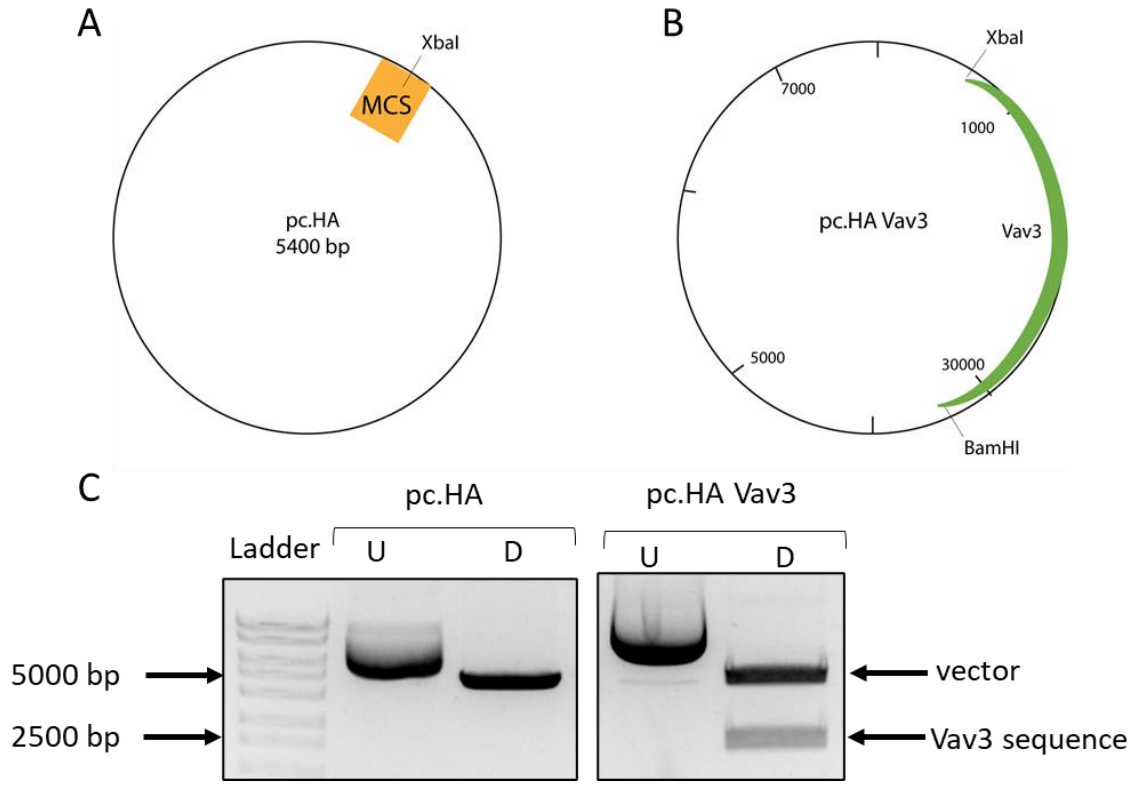

Figure 13. Digestion of plasmids pC. HA and pC.HA Vav3. (A) Schematic representation of the pC.HA vector. The multi cloning site (MCS) and the localization of BamHI recognition site are indicated. (B) Schematic representation of the pC.HA Vav3 plasmid. The insert corresponding to the Vav3 encoding sequence (green portion) and the recognition sites for XbaI And BamHI are indicated. (C) Agarose gel displaying the results of the digestions performed. Undigested vectors (U) migrate at higher molecular weight. Digested vectors (D) migrate as the linearized conformation and are more accurate to determine the size of the bands.

To further evaluate if the pC.HA Vav3 plasmid is suitable for Vav3 overexpression in mammalian cells, we transfected human epithelial HeLa cells with pC.HA and pC.HA Vav3 and analyzed by western blot the expression of Vav3-HA using an anti-HA antibody. Western blot on total protein extracts of HeLa cells either non-transfected (NT) or transfected with the pC.HA or with the pc.HA Vav3.

In cells transfected with pC.HA Vav3 we detected a protein band at a molecular weight of about 100 kDa (Figure 14), which is compatible with the molecular weight of Vav3 (98 kDa). We also detected a band at a lower molecular weight which may correspond to a product of

degradation of Vav3 -HA or to a non-specific detection. No bands were detected in the total lysates of NT or pC.HA-transfected cells. To control that every lane in the gel were loaded with protein lysates we used an anti-actin antibody. Actin was detected in all the lanes indicating that the absence of HA-specific bands is not related with the absence of protein (Figure 14). These data show that pC.HA Vav3 is suitable to express Vav3-HA in mammalian cells.

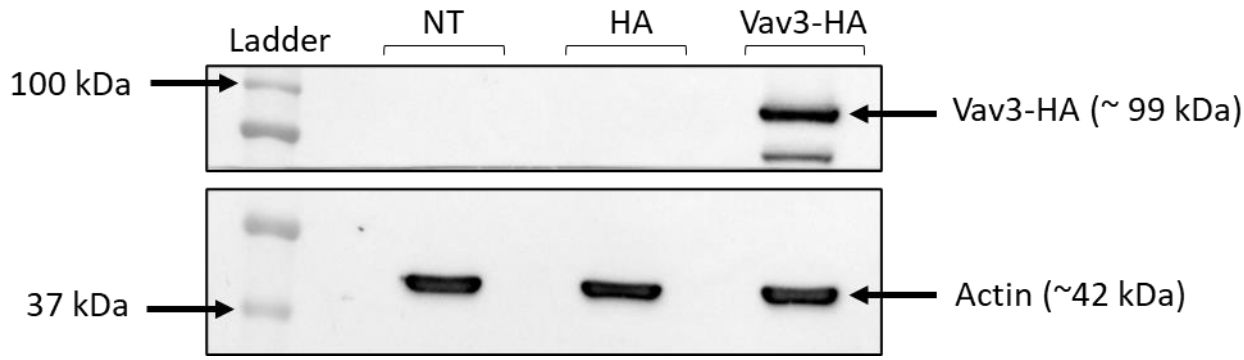

Figure 14. Western blot analysis on total lysates of HeLa cells in non-transfected (NT) or transfected (HA and Vav3-HA) conditions. The expression of Vav3-HA was detected using an anti-HA antibody. Ladder and corresponding molecular weights are shown. Actin was used as loading control.

3.2 Optimization of transfection conditions

Given that the subsequent experiments need to be performed in cell populations with high percentage of transfected cells, we tested growing DNA concentrations to transfect HeLa cells and evaluate the percentage of cells expressing Vav3-HA by immunofluorescence microscopy.

HeLa cells were transfected followed the polypolus-DNA transfection protocol. The day after transfection cells were fixed and processed for immunofluorescence. The expression of HA and Vav3-HA was detected by using an anti-HA antibody. Cells were also labelled with DAPI to detect the nucleus and with phalloidin which allows actin detection. Representative fluorescence microscopy images are shown in Figure 15.

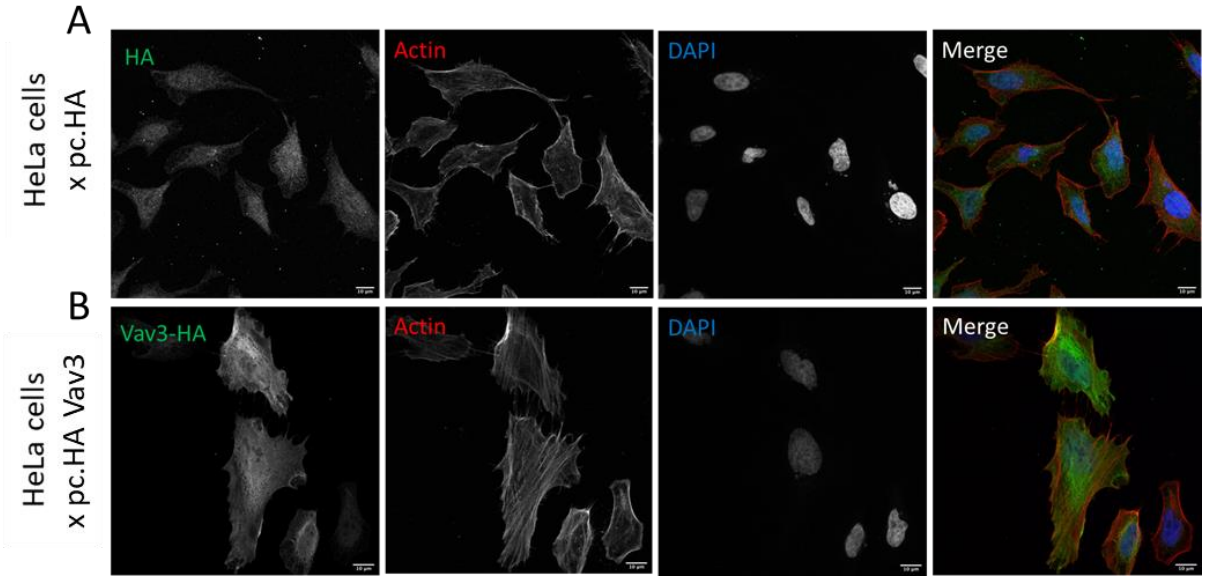

Figure 15. Immunofluorescence microscopy images of HeLa cells transfected with (A) pC.HA or (B) pC.HA Vav3. Cells were immunolabelled with primary antibody HA raised in mouse (green) and labelled with phalloidin coupled to AlexaFluor 647 (red) and DAPI (blue). Images were collected with a Leica SP5II confocal laser-scanning microscope equipped with a 63 × 1.4 NA objective and processed using ImageJ.

To assess the percentage of transfection approximately 200 cells from 10 independent fields were quantified. The percentage of transfection was calculated dividing the number of cells HA-positive cells by the total number of cells as quantified by DAPI staining. The percentage of transfected cells detected for each DNA concentration tested is displayed in Figure 16. This graph shows that the highest percentage of Vav3-HA expressing cells, about 66% of the entire population (Figure 16), was obtained when transfection is performed with 2 µg of DNA.

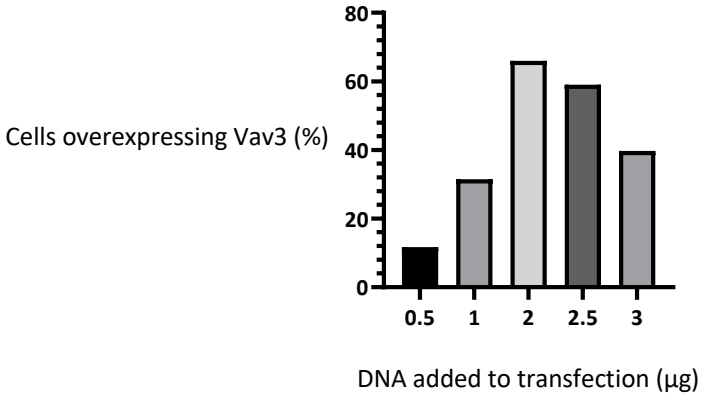

Figure 16. Graph showing the percentage of cells expressing Vav3-HA in response to the use of growing amounts of DNA in the transfection protocol. These data were obtained by the quantification of immunofluorescence microscopy images similar to those shown in Figure 15.

3.3 Effect of Vav3 overexpression in LLO-intoxication of HeLa cells

Having found the optimal conditions to transfect HeLa cells to have the highest percentage of cells overexpressing Vav3, we tested the effect of Vav3 overexpression in LLO intoxication. For that we intoxicated the cells with purified LLO 24 h after transfection and evaluate the permeability of the PM membrane by PI permeability assays. Cells are normally impermeable to PI however they become permeable if the PM undergoes damage as it is the case upon LLO pore formation (Figure 17A). Damaged cells which turn PI-positive were detected by flow cytometry. We used HeLa cells in non-transfected (NT) conditions and Hela cells expressing either HA or Vav3-HA, which we intoxicated with increasing doses of LLO ranging from 0.05 to 0.5 nM.

For all the cells tested (NT, HA or Vav3-HA), we observed that the percentage of PI-positive cells increase in a dose-dependent manner in response to growing concentrations of LLO (Figure 17B). However, the percentage of PI-positive cells was significantly lower in the populations of cells overexpressing HA or Vav3-HA (Figure 17B), suggesting that the transfection procedure might be interfering with the intoxication. Non-intoxicated cells display the same level of PI permeability (15 % of PI-positive cells) in all the cell populations tested.

While the permeability to PI in HA- and Vav3-HA expressing cells is similar at lower concentrations of LLO (0.05 to 0.20 nM), at 0.5 nM LLO Vav3-expressing cells are significantly less permeable to PI (Figure 17B), suggesting that at higher LLO concentrations Vav3 overexpression might act as a protective factor to PFT damage.

These data suggest a role for Vav3 to limit the damage induced by LLO specifically at concentrations higher than 0.50 nM. In addition, in these experiments at a concentration of 0.50 nM LLO HeLa cells NT or expressing HA start to die upon intoxication while cell death is decreased in Vav3-expressing HeLa cells.

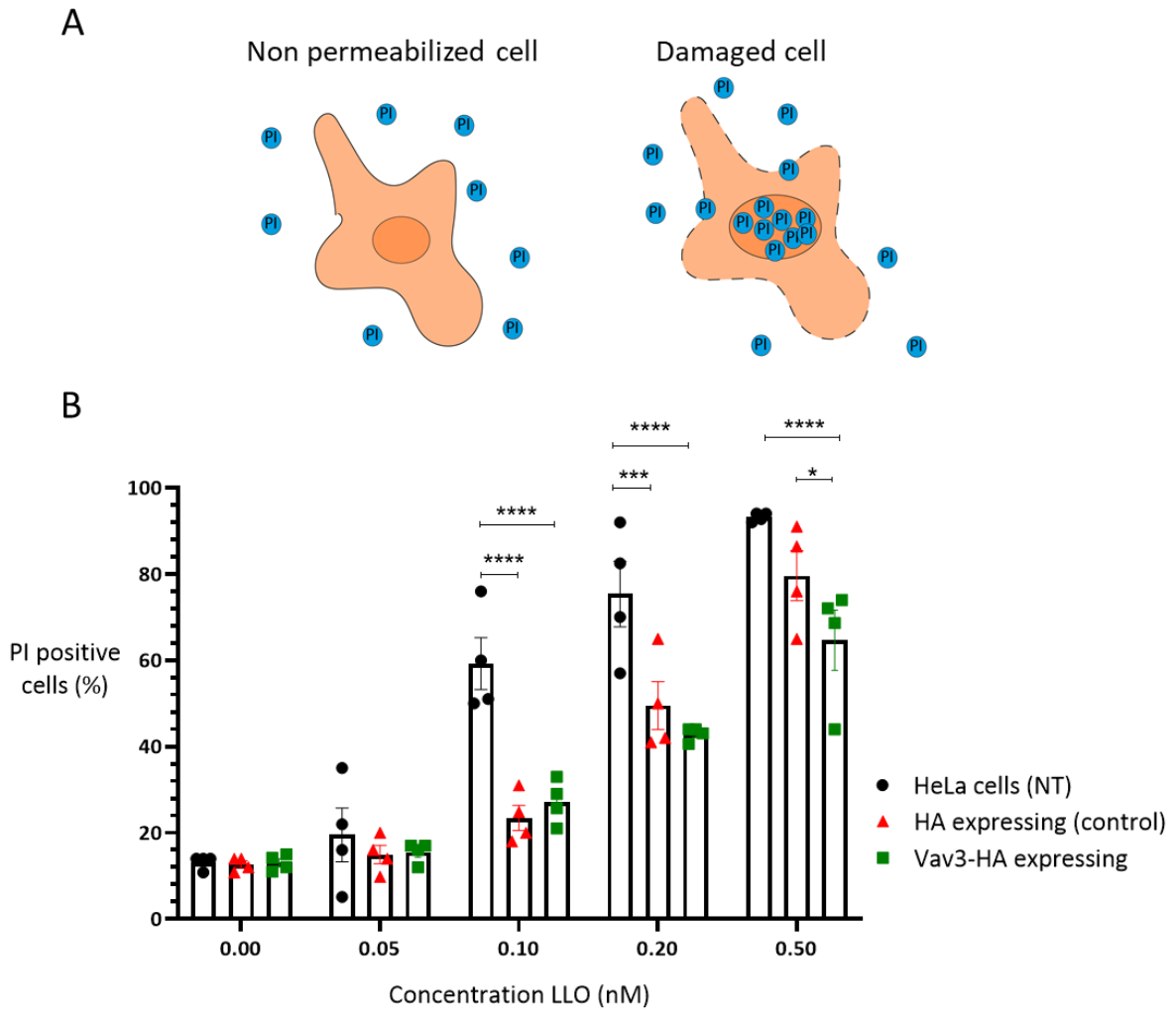

Figure 17. PI permeability assay in response to increasing concentrations of LLO in HeLa cells non-transfected (NT) or transfected to express either HA (control) or Vav3-HA. PI-positive cells were detected by flow cytometry. Data show the result of 4 independent experiments, values are the mean ± SEM (n=4); p-values were calculated using two-way ANOVA with multiple comparations. For statistically significant differences: * $p \leq 0.05$; *** $p \leq 0.001$; **** $p \leq 0.0001$.

3.4 Effect of Vav3 overexpression in the recovery upon LLO intoxication

Taking into account that the overexpressin of Vav3 does not significantly increase the resistance to PM damage induced by in sub-lytic doses of LLO, we wonder if Vav3 overexpression would promte the recovery of PM integrity upon LLO intoxication. For that, we intoxicated HeLa cells expressing (HA or Vav3-HA) with the 0.2 nM LLO for 20 min, washed out the unbound toxin and allow cells to recover. At different times of recovery ranging from 0 to 6 h, cells were processsed for PI permeability assays and analysed by flow cytometry.

As previously noticed (Figure 17), in non-intoxicated conditions, cells expressing HA behave similarly to those expressing Vav3-HA concerning their permeability to PI. Only 10% of the cells are PI-positive and this value is maintained along time (Figre 18). Upon incubation with 0.2 nM LLO for 20 min (0 h) HA and Vav3-HA expressing cells are damage and 35 % of the become permeable to PI (Figure 18). After 2 h of LLO wash out, the percentage of PI positive cells drop to 20 % and no further recovery was detected along the time of recovery. As shown in Figure 18 ,HA and Vav3-HA-expressing cells behave similarly concerning the recovery of PM integrity.

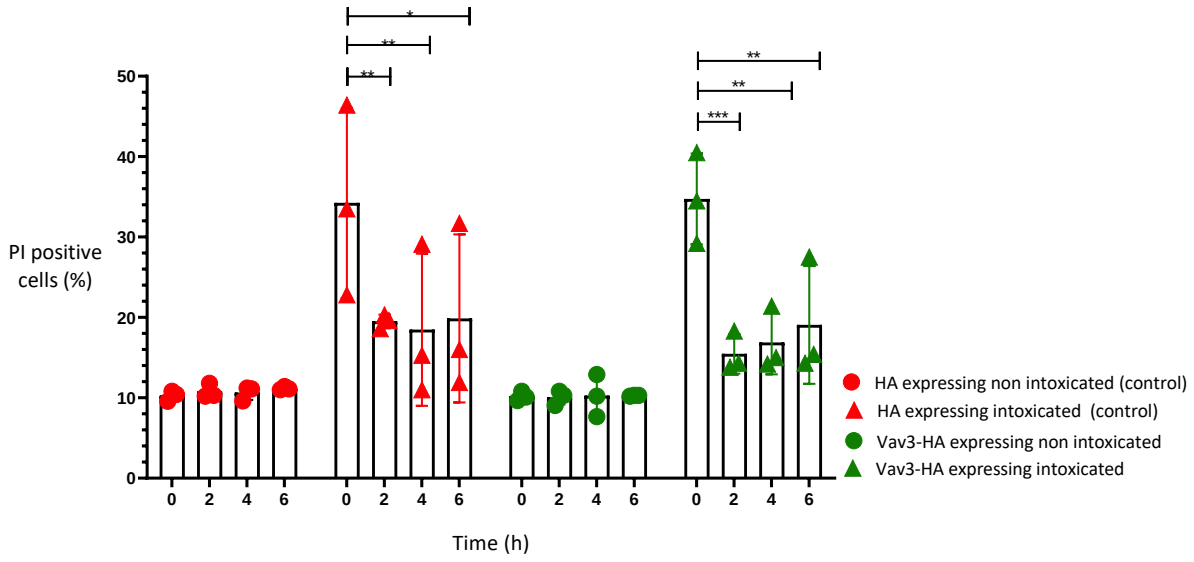

Figure 18. PI permeability assay during the recovery of LLO-induced PM damage in HeLa cells overexpressing either HA (control) or Vav3-HA. Cells were intoxicated with 0.2 nM LLO during 20 min and LLO was washed out to allow repair. Permeability of the PM was quantified by flow cytometry following PI incorporation right after intoxication (0 h) or overtime of recovery (2, 4 and 6 h). Graph shows quantifications of PI-positive cells obtained from flow cytometry plots of non-intoxicated (green and red circles) or intoxicated samples (red and green triangles). Values are the mean ± SEM (n = 3); p-values were calculated using two-way ANOVA with multiple comparations. For statistically significant differences: * $p \leq 0.05$; ** $p \leq 0.01$; *** $p \leq 0.001$; **** $p \leq 0.0001$.

Data obtained suggest that Vav3-HA has no role in the recovery from PM damage induced by sub-lytic doses of LLO. In addition, our results indicate that 2 h after LLO wash out both HA and Vav3-HA expressing cells reach their maximum recovery capacity, as no additional decrease in PI positive cells was detected at later time points. However, this experiment has the limitation that the whole cell population is not transfected and thus the cells that do not express Vav3-HA may mask a possible effect of Vav3 in the resistance of cells to intoxication.

3.5 Construction and verification of Vav3-GFP fusions

To overcome the limitation of analyzing mix populations of Vav3-HA expressing and non-expressing cells, we designed new constructs from which Vav3 is expressed in fusion with a GFP-tag. The cells expressing GFP can be separated in FACS and analyzed independently from the cells that do not express GFP, and thus would allow to assess the effect of Vav3 in intoxication and repair from damage. For this we obtained from Professor L. Burnstein (USA) three plasmids encompassing different Vav3 encoding variants (Figure 19): the wild type sequence (Vav3-WT), a sequence encoding an inactive Vav3 having 3 mutations in the GEF domain (Vav3-ISO) and a sequence encoding a Vav3 that is not able to bind PM lipids and only acts in the cytoplasm (Vav3-W943L). These plasmids were used as template to sub-clone the different Vav3 sequences in fusion with GFP in another plasmid.

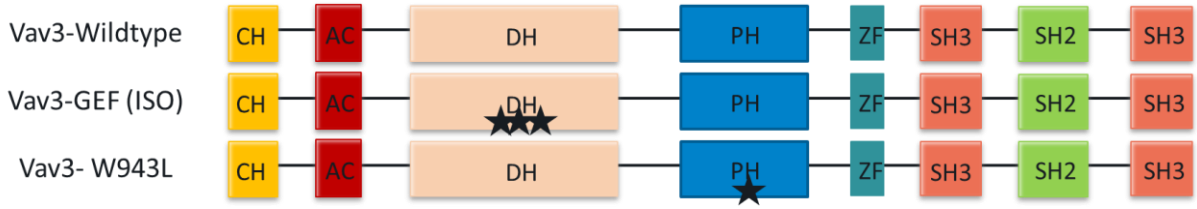

Figure 19. Schematic representation of Vav3 variants including the eight different domains and the specific mutations affecting their activity or PM targeting. Vav3-ISO has three point mutations given rise to 3 amino acids substitutions in the DH domain. These mutations abrogate its GEF activity. Vav3-W493L has a point mutation in the PH domain enabling its interaction with the PM while maintaining GEF activity in the cytoplasm.

First, we confirm the nature of the plasmids obtained. Purified plasmids were used in a digestion reaction with the restriction enzymes EcoRI and SalI, which were the ones used to clone the inserts in the pIRES vector. As expected, we obtained two fragments (Figure 20): the vector backbone pIRES (6.1 Kb) and the insert corresponding to the Vav3 sequences (2.5 Kb).

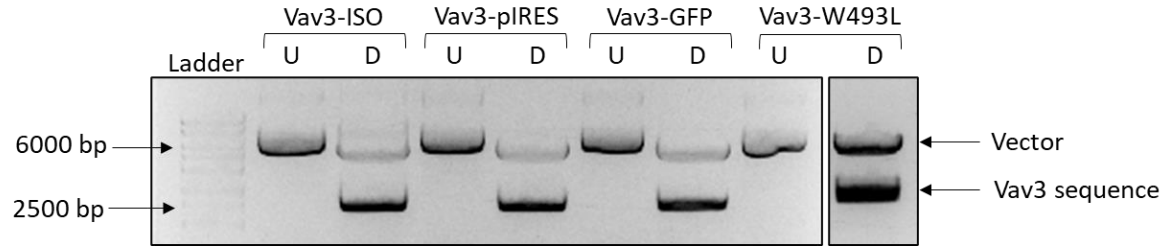

Figure 20. Digestion of Vav3 plasmids obtained from Professor L. Burnstein. Agarose gel (1 %) displaying the results of the simultaneous digestion by EcoRI and SalI. Undigested vectors (U) migrate as a single band at higher molecular weight. Lanes containing the samples of the digested vectors (D) display two bands, the vector backbone and the excised Vav3-encoding inserts.

These data suggest that the plasmids were correct. To further confirm the presence of the described mutations, the vectors were sent for DNA sequencing. The data obtained definitively allowed us to validate the nature of the inserts and the presence of the mutations.

The sequences encoding Vav3-WT, ISO and W493L were amplified by PCR using the original plasmids as template and the oligonucleotides Primer 3 and Primer 4 (Table 2). The PCR products were run in an agarose gel to assess their size, their integrity and the specificity of the amplification. A single band at the expected molecular weight was detected (Figure 21A). The obtained DNA amplification fragments were ligated in the vector pEGFP-N2 at EcoRI and SalI restriction sites (Figure 21B, C) to obtain a fusion with GFP, which is located at the C-terminus of Vav3 sequences (Figure 21C).

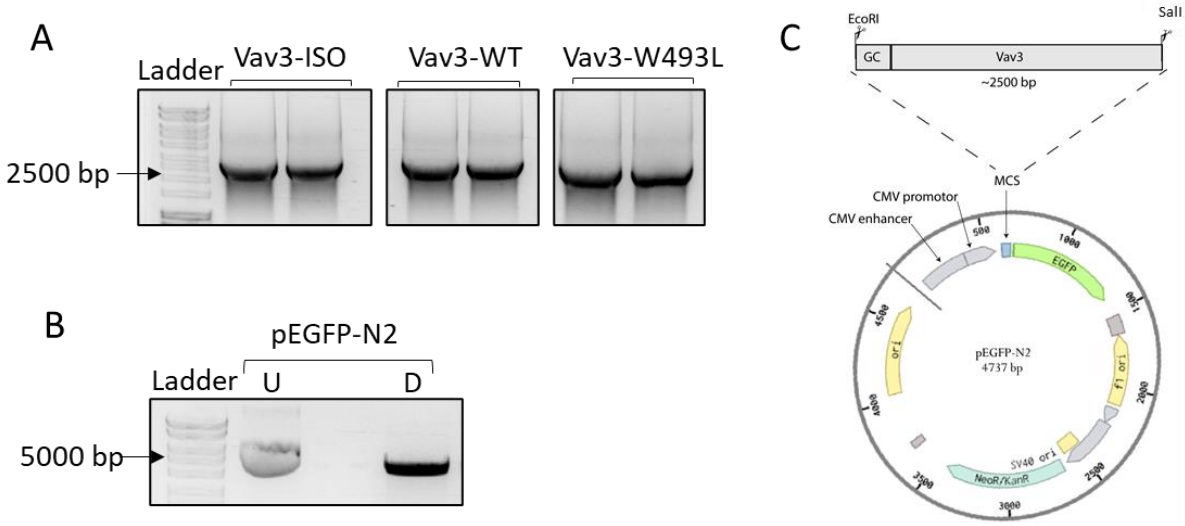

Figure 21. Construction details of Vav3-GFP fusions. (A) Agarose gel showing the DNA fragments encoding Vav3-ISO, Vav3-WT and Vav3-W493L, amplified by PCR. (B) Agarose gel displaying undigested pEGFP-N2 (U) and digested pEGFP-N2 (D) with EcoRI and SalI. (C) Schematic representation of the insertion of Vav3 sequences (WT or ISO or W493L) in the MCS of pEGFP-N2 previously digested by EcoRI and SalI.

E. coli colonies obtained after transformation with the ligated plasmids were tested by colony-PCR for the presence of pEGFP-N2 containing the Vav3 inserts. For that we used primer 1 (in insert) and 6 (in plasmid) (Table 2) for PCR amplification (Figure 22A). In samples with positive colonies a band of 372 bp should be detected (Figure 22B).

Figure 22. Verification of grown colonies by colony PCR. (A) Schematic representation of a positive clone. The site of annealing for Primer 1 and 6, as well as the direction of the amplification, are indicated. (B) Products of PCR reaction using the primers 1 and 6 were run in an agarose gel. Colonies 1 to 4 correspond to Vav3-ISO-pEGFP-N2, colonies 5 to 8 to Vav3-WT-pEGFP-N2 and colonies 9 to 12 to Vav3-W493L-pEGFP-N2. The colonies used to pursue our studies are the ones encircled in green (1, 5 and 9).

As expected, all the PCR amplifications generate a band of approximately 400 bp, confirming the presence of the insert in all the colonies tested. Colonies 1, 5 and 9 were selected to pursue our studies. The corresponding plasmids were purified, sent for DNA sequencing and used to perform other verifications. Table 4 show the concentration of each plasmid obtained after purification.

Table 4. Quantification of DNA concentration and purity of purified plasmids. Values were obtained in a Nanodrop equipment. The ratio between abs 260/280 of approximately 1.8 is generally accepted as "pure" for DNA. The ratio between abs 260/230 are commonly in the range of 2.0-2.2. These results provided by ratios between abs 260/280 and 260/230 are accepted as pure for all Vav3 constructions (WT or ISO or W493L)

Construct	Concentration (ng/µL)	Abs 260/280	Abs 260/230
Vav3-WT-pEGFP-N2	415.40	1.84	1.74
Vav3-ISO-pEGFP-N2	673.50	1.85	1.88
Vav3-W493L-pEGFP-N2	685.80	1.84	1.67

To further verify the clones obtained, the purified plasmids were used in another PCR amplification using the oligonucleotides Primer 2 (in the insert) and the 7 (in the vector) (Table 2) (Figure 23A). The expected size of the fragment amplified with this pair of oligonucleotides is 699 bp. As negative control we used the vector pEGFP-N2, from which a lack of amplification was expected. In agreement, in samples containing the plasmids Vav3-WT-pEGFP-N2, Vav3-ISO-pEGFP-N2 and Vav3-W493L-pEGFP-N2 we detected a band at the expected size while no

bands were detected in the control PCR reaction using pEGFP-N2 as template (Figure 23B). In addition, the same plasmids were digested Sac1, which is located in the MCS of pEGFP-N2 and thus cuts the plasmids at a single position. All the plasmids were successfully linearized by Sac1 (Figure 23C), the empty pEGFP-N2 migrated under 5000 bp which is compatible with its size (4737 bp) and the plasmids harboring Vav3 sequences migrate between 8 kb and 6 kb, which corresponds to the expect size for pEGFP-N2 containing Vav3 sequences (2500 bp).

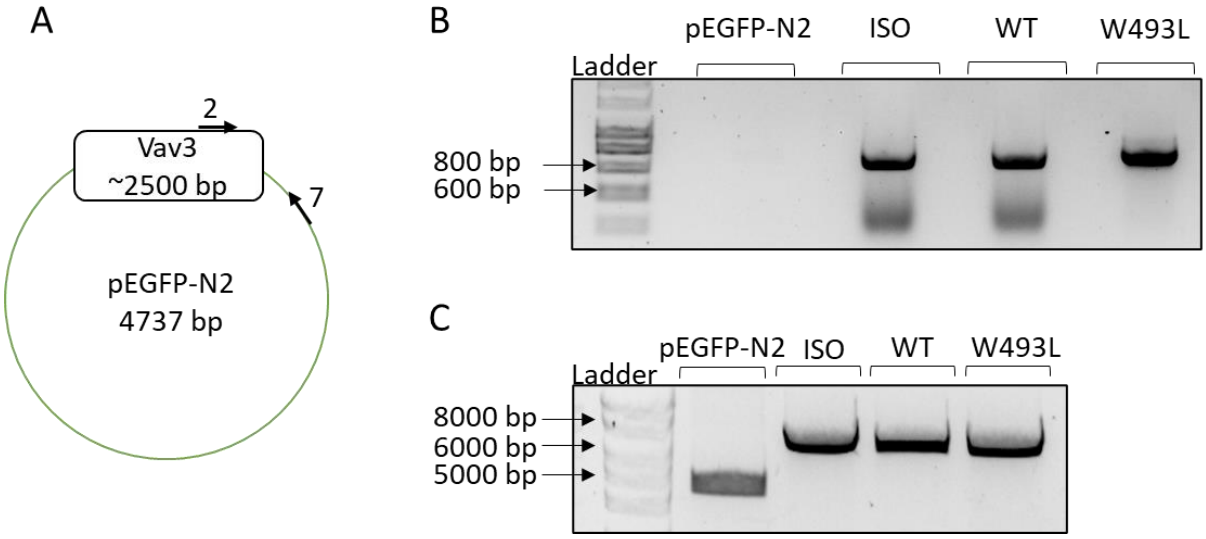

Figure 23. Further confirmation of the selected clones. (A) Schematic representation of a positive clone. The site of annealing for Primer 2 and 7, as well as the direction of the amplification, are indicated. (B) Products of PCR reaction using the primers 2 and 7 were run in an agarose gel. Molecular weight is indicated. (C) Agarose gel of the digestion of the different plasmids by Sac1.

These data, together with the full sequencing of the inserts and their junction with the vector definitively confirm the successful cloning of each Vav3 variant in fusion with GFP. The presence of the mutations ISO and W493L was also verified and confirmed by sequencing. No additional mutations were detected.

These constructs should allow the expression of Vav3 in fusion with GFP. To confirm that, we transfected HeLa cells with the different plasmids and evaluate GFP expression by several approaches: immunofluorescence microscopy, flow cytometry and western blot on total cell lysates.

After transfection, cells were fixed and processed for immunofluorescence. Besides the detection of GFP cells were also labelled with DAPI to detect the nucleus and with

phalloidin which allows actin detection. Representative fluorescence microscopy images are shown in Figure 24.

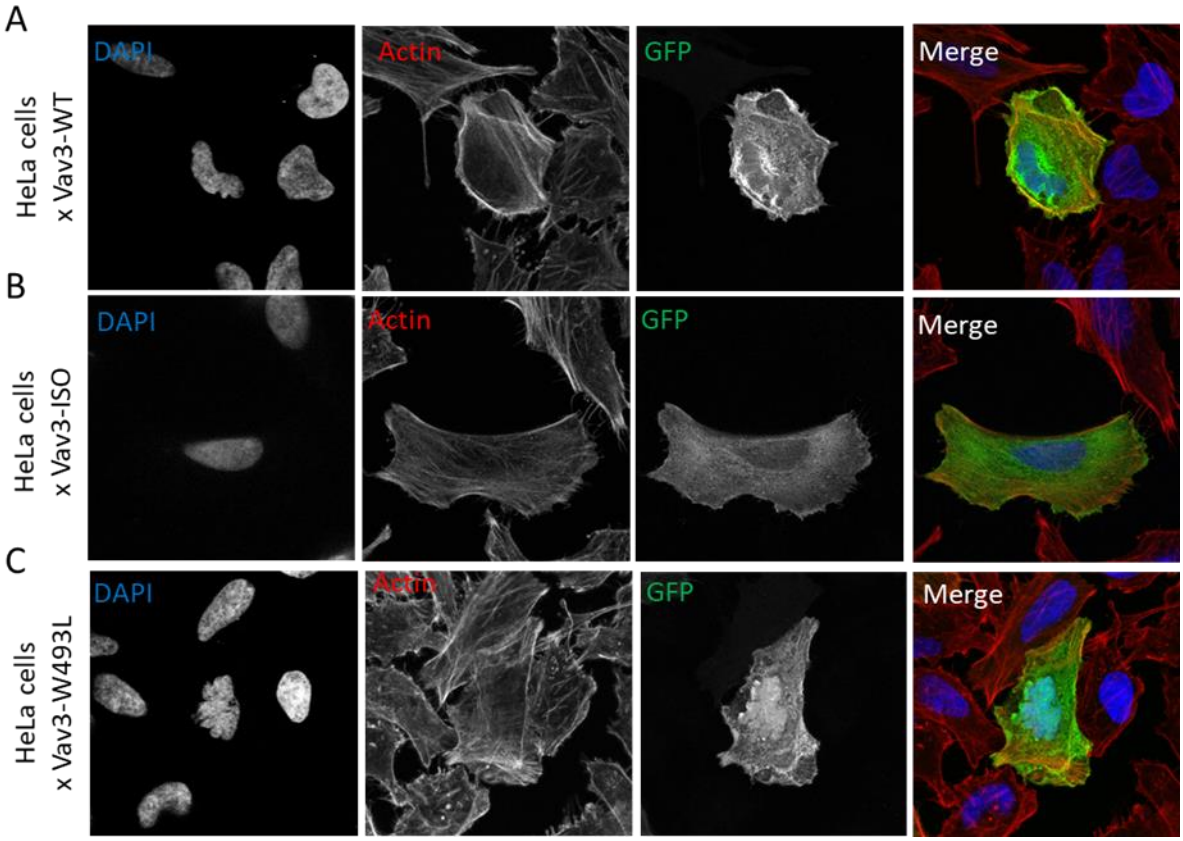

Figure 24. Immunofluorescence microscopy images of HeLa cells transfected to express (A) Vav3-WT (B) Vav3-ISO or (C) Vav3-W493L. Cells were labelled with phalloidin coupled to AlexaFluor 647 (red) and DAPI (blue). Images were collected with a Leica SP5II confocal laser-scanning microscope equipped with a 63 × 1.4 NA objective and processed using ImageJ.

The flow cytometry analysis of the full population of cells allowed us to evaluate the percentage of GFP-expressing cells, and thus to evaluate the percentage of transfected cells (Figure 25A, B). HeLa cells (NT) were used as negative control and served to determine the threshold of GFP expression. In the transfection conditions used, 35 % of the cell population were GFP-positive, indicating that 35 % of the cells were transfected (Figure 25A, B). We finally assess GFP expression by western blot on total cell lysates of HeLa cells transfected with the different plasmids using a specific antibody that recognizes GFP (Figure 25C). The antibody revealed a band above 100 kDa, which may correspond to the molecular weight of the fusion Vav3 (98 kDa) with GFP (27 kDa).

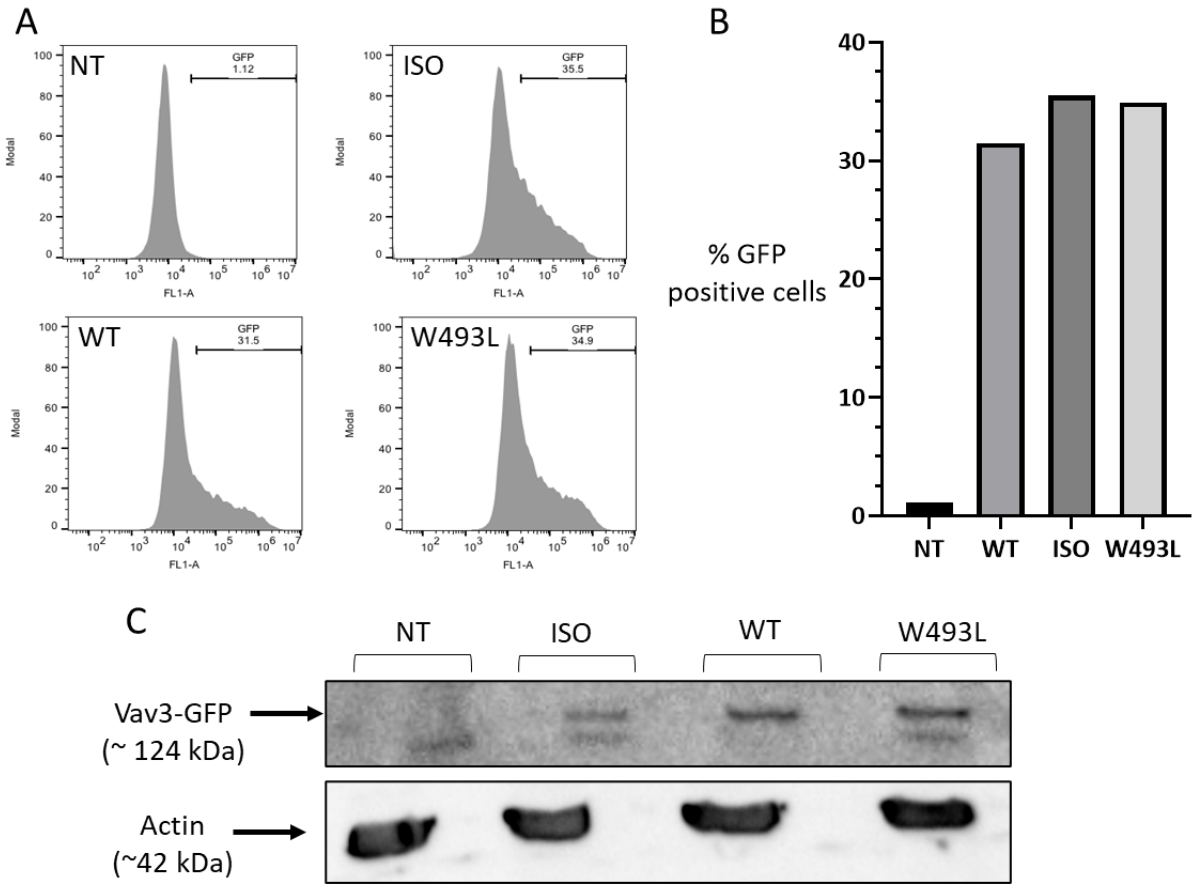

Figure 25. Confirmation of the expression of GFP in transfected cell populations. (A) Flow cytometry assays. Flow cytometry plots showing the percentage of GFP-positive cells. (B) Graphic representation of the percentage of GFP in non-transfected cells (NT) and HeLa cells expressing Vav3 variants in fusion with GFP (ISO or WT or W493L). (C) Western blot analysis on total lysates of HeLa cells in non-transfected (NT) or transfected (Vav3-ISO or Vav3-WT or VAv3-W493L) conditions. The expression of Vav3-GFP was detected using an anti-GFP antibody. Corresponding molecular weights are indicated. Actin was used as loading control.

Altogether, these data indicate that the Vav3-GFP variants are correctly constructed and are correctly expressed in cells, and thus they can be used to test the effect of Vav3 overexpression in intoxication and repair upon PM damage. In addition, the activity (ISO) and localization (W493L) mutants will allow to test their specific role in response to PFTs.

3.6 Effect of LLO-intoxication in the expression of endogenous *vav3*

Considering that the protein Vav3 could be important in the response to intoxication and may have a protective role against PFT-induced PM damage, we wondered if cells would increase the expression of endogenous *vav3* upon LLO intoxication or during damage recovery. To assess this issue, we intoxicated HeLa cells with sub-lytic doses of LLO (0.2 nM

LLO) for 20 min, washed out the unbound toxin and allow cells to recover. Total RNA was extracted from cells at different times of recovery ranging from 0 to 6 h. The expression of *vav3* was evaluated at each time point by qPCR after reverse transcription.

Purified RNAs were first analyzed to assess RNA integrity and purity. Each sample was analyzed by three methods: Abs measurement in NanoDrop (Table 5), Experion (Figure 26) and agarose gel-electrophoresis (Figure 27).

Table 5. Qualification of RNAs concentration an assessment of RNA purity, obtained by Nanodrop. Ratio between the absorvance (Abs) at 260 and 280 gives an indication about contamination with protein, the values should be near to 2.0 to neglect any protein contamination. Ratio between the absorvance (Abs) at 260 and 230 gives an indication about contamination by reagents, values from 2.0 to 2.2 are accepted

Samples	Concentration (ng/µL)	Abs 260/280	Abs 260/230
NI (0 h)	449.10	1.98	2.10
I (0 h)	462.10	1.97	2.42
I (2 h)	347.90	1.98	2.45
I (4 h)	403.50	2.04	2.08
I (6 h)	378.30	1.96	2.44

To verify the integrity of RNA, the samples were run in Experion and separated by agarose gel electrophoresis. Data from Experion (Figure 26) allowed the detection of the bands corresponding to the 28S and 18S ribosomal RNA subunits for all the samples (Figure 26A), which could be quantified as distinct peaks. No RNA degradation was detected.

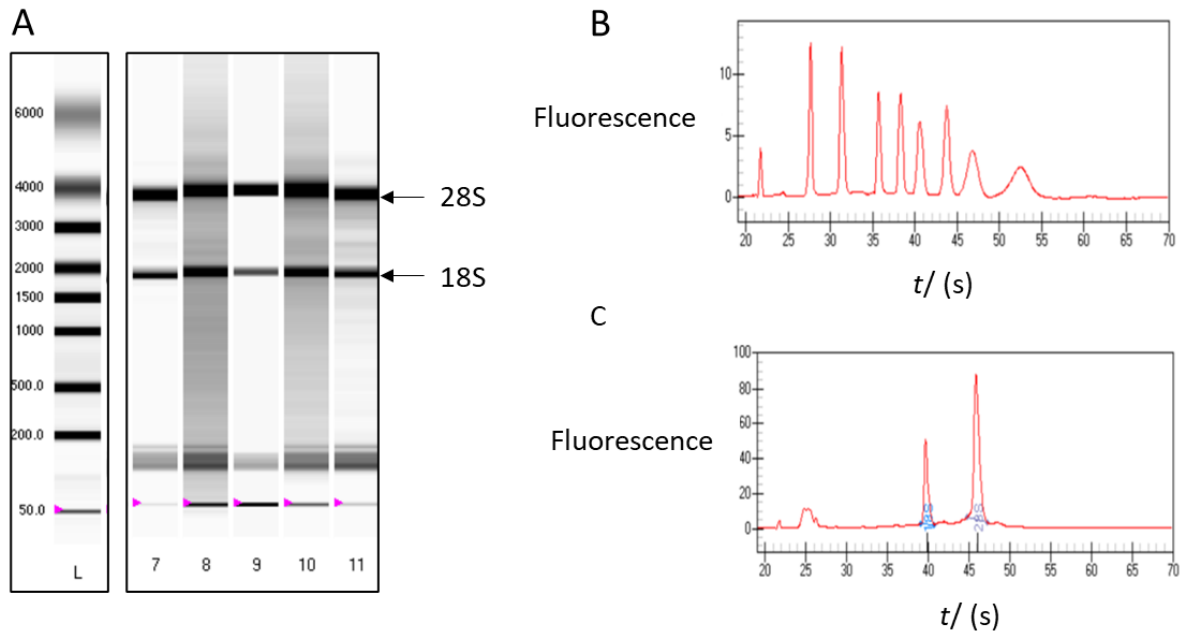

Figure 26. RNA quality assessed by an Experion electrophoresis system. (A) Image from gel electrophoresis obtained by Experion. Bands corresponding to 28 S and 18 S ribosomal RNAs are indicated. (B) Ladder florescence profiles obtained by Experion. (C) Fluorescent profile of the sample non-intoxicated obtained by Experion.

As a complement we also analyzed the RNA samples by agarose gel electrophoresis. This alternative technique also allows to evaluate RNA quality and integrity (Figure 27). Confirming the results obtained by the Experion analysis, we detected discrete bands at the molecular weight of the 18S (1.9 Kb) and 28S (5 Kb) ribosomal RNAs, indicating the integrity and the purity of the samples.

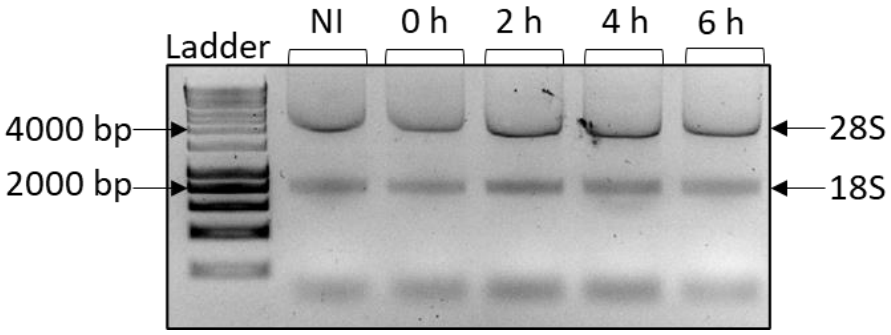

Figure 27. Agarose gel after the electrophoresis of RNA samples. A ladder was used to determine the approximate molecular weight of the detected bands. The bands corresponding to the 18S and 28S ribosomal RNAs are indicated.

Altogether these analyses indicate that our purified RNA samples have a suitable degree of purity and integrity and can be used in further experiments to evaluate *vav3*

expression. Thus, 1 µg of RNA for each sample was converted into cDNA by reverse transcription.

We first performed calibration curves with the specific primers (Table 3) for *vav3* and *hprt1* (control housekeeping gene) to determine the ideal concentration of cDNA to be used in the qPCR (Figure 28). The standard curve is constructed by plotting the log of the starting quantity of template against the CT value obtained during each amplification. The equation of the linear regression line, along with Pearson's correlation coefficient (r) or the coefficient of determination (R^2), can then be used to evaluate whether your qPCR assay is optimized.

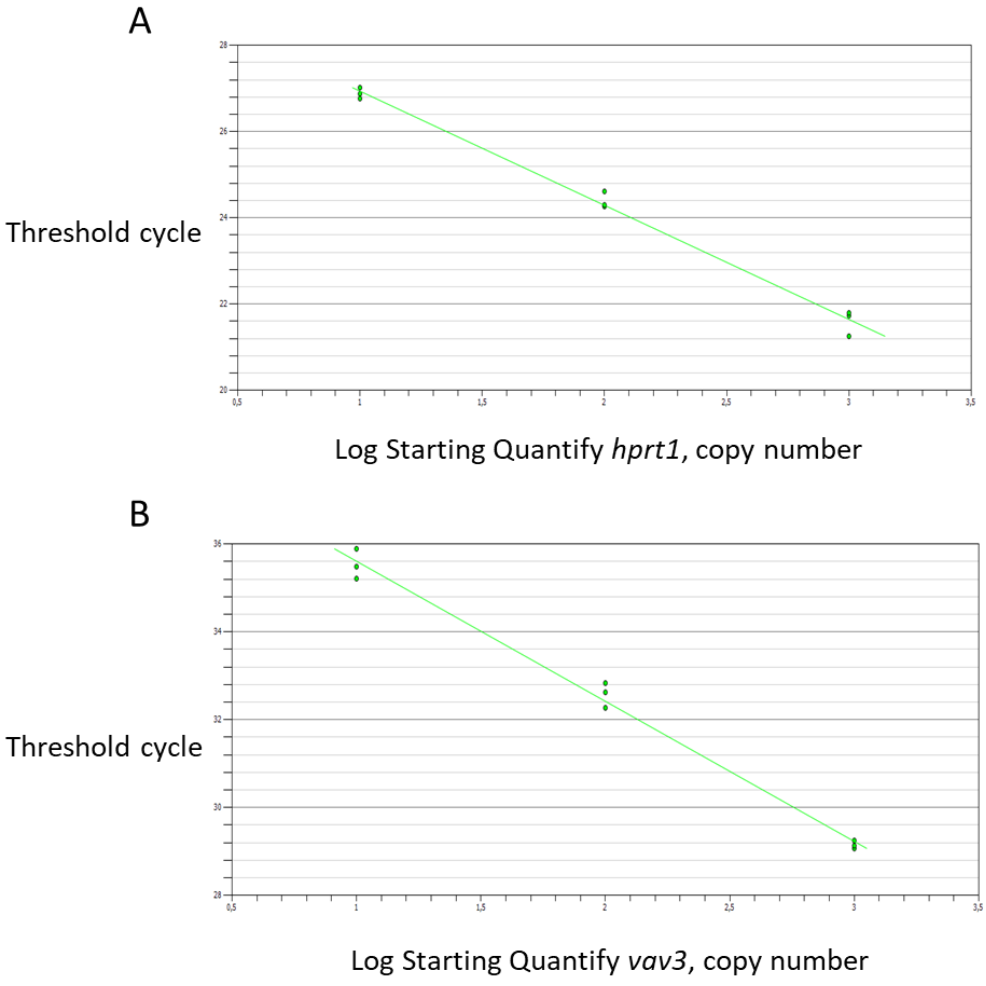

Figure 28. Calibration curves to determine the concentration of cDNA to use. (A) Calibration curve for *hprt1*, control housekeeping gene. (B) Calibration curve for *vav3*.

Having determined the cDNA concentration to be used, we assessed the expression of *vav3* and *hprt1* in the different samples. Data obtained for *vav3* was normalized to the values obtained for *hprt1*, which is used as control and whose expression is not expected to vary in response to intoxication or during repair. The expression of *vav3* does not significantly vary in

response to intoxication nor during the first ours of recovery (Figure 29A). However, at 6 h of recovery a slight significant decrease in *vav3* expression was detected (Figure 29A). We also performed the analysis by normalizing the data by the values obtained from non-intoxicated cells, in that case no significant variation in *vav3* expression were detected (Figure 29B).

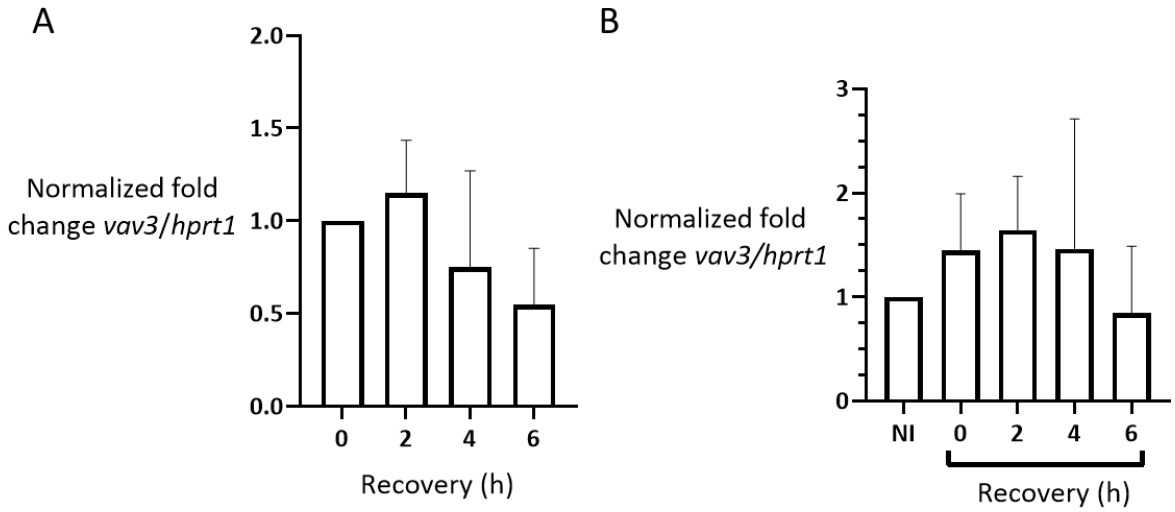

Figure 29. Expression of endogenous vav3 in response to intoxication and during recovery. (A) Expressing of *vav3* normalized to *hrpt1* (housekeeping gene) and cells upon intoxicated (0 h). (B) Expressing of *vav3* normalized to *hrpt1* (housekeeping gene) and non-intoxicated cells (NI).

These data indicate that the intoxication of HeLa cells with sub-lytic LLO concentrations do not alter the expression of *vav3*. In addition, *vav3* expression is not altered during the recovery from damage induced by sub-lytic doses of LLO.

4. DISCUSSION

PFTs permeabilize host cells, typically by targeting the PM[128]. LLO is a potent PFT, expressed and secreted by *Listeria monocytogenes* (*Lm*)[129]. LLO monomers bind to cholesterol in host cell PM and oligomerize to form large complex pores[130], through which massive calcium influx takes place. Calcium is a key messenger strictly required for PM repair[131]. Rapid PM repair is crucial for cell survival, but the molecular mechanisms deployed by cells to maintain membrane integrity remain poorly understood.

From previously studies, our investigation group hypothesized that if a host protein is important to resist intoxication by PFTs, cells with increased expression of that specific protein would be more resistant. In this context, to identify new proteins important for PM repair and cell survival to intoxication, a gain-of-function approach was used in a full genetic screen. The gene encoding the Guanine Nucleotide Exchange Factor Vav3 emerged as a strong candidate involved in the response to PFTs. Thus, this dissertation focused on the role of Vav3 in the repair of LLO-induced PM damage.

In the screen, cells that overexpress the sequence encoding Vav3 appeared to survive to lytic concentrations of LLO. To validate this result, we overexpressed Vav3 in HeLa cells, using a mammalian overexpression vector, and evaluate if expressing Vav3 from that vector confer more resistant to LLO intoxication. Our data show that, when intoxicated with low doses of LLO, Vav3 overexpressing cells behave similarly to control cells (transfected with the empty vector). However, at higher concentrations, where some cell death starts to occur, Vav3 overexpression cells appeared to be slightly more resistant to LLO-induced damage. These data suggested that while the overexpression of Vav3 does not represent an advantage in resistance to sub-lytic doses of LLO-intoxication, at higher concentrations the overexpression of Vav3 may protect cells from cell death. To assess the possible role of Vav3 overexpression during the recovery from sub-lytic damage cells were intoxicated and analyzed at several time points after LLO-washout. Our data demonstrate that control and and Vav3-expressing cells behave similarly concerning in the recovery of PM integrity which mean that expressing Vav3 does not confer any advantage in repair. However, this experiments were performed in mixed cell populations which we know to include at best 60 % of cells transfected cells, and thus at least 40 % of the cells do not overexpress Vav3. In our experimental setup, the cells overexpression Vav3 could not be separated from the full population, which might

represent a major weakness in our analysis, as a possible effect of Vav3 overexpression may be masked by non-transfected cells in the population. To overcome this problem, we designed and constructed new expression vectors that allow the expression of Vav3 in fusion with a GFP tag. The fluorescence of the GFP tag should allow us to identify and separate the cells overexpressing Vav3 during FACS analysis and specifically analyze the damage in these cells undermining the contribution of the non-transfected cells in the analysis. Another issue that we need to consider from the data obtained, is that the gain-of-function screen was performed under lytic concentrations of LLO and it is possible that Vav3 only plays a role in such extreme conditions. In the future we need to investigate the role of Vav3 under higher LLO concentration, which may represent a challenge as the percentage of death cells will increase.

Interestingly, high levels of Vav3 have been observed in various types of cancer, including glioblastoma[132] and prostate cancer[133]. Studies revealed that Vav3 oncogene is overexpressed in human prostate cancer, enhances androgen receptor (AR)-mediated signaling, and may play a role in prostate cancer development and progression[134]. In addition, it has been shown that cancer cells, especially migratory cancer cells, display an upregulation of the PM repair mechanisms [135] suggesting that Vav3 could play a role in the repair of the damaged PM. It is thus expected that, Vav proteins exert disease-specific tasks that are unrelated to their normal function in healthy tissues. Under disease or stress conditions, the cell may directly increase Vav3 expression to respond to a specific condition.

Taking this into account, we postulated that upon intoxication the cell may respond to the damage by directly increase the transcription of the Vav3 encoding gene, thus increasing *vav3* mRNA and ultimately increasing Vav3 protein levels. To assess that, we evaluated by RT qPCR the levels of *vav3* mRNA in response to LLO intoxication and during PM recovery from damage. Our data indicated that the expression of *vav3* remains unchanged during the recovery. Given these results, one might speculate that even if the expression of Vav3 is not affect by intoxication, the levels of activation of Vav3 and its recruitment to the PM may be increased upon intoxication and might be sufficient to mount an efficient response to the damage inflicted. The levels of activation or the cellular localization of Vav3 were not addressed here but might be included in future studies.

5. CONCLUSION

The data reported in this dissertation show that overexpressing Vav3 does not confer an advantage in cell resistance to sub-lytic LLO doses and also indicate that under such conditions, cells do not increase the expression of *vav3*. However, the results suggest a role for Vav3 in the response to lytic concentrations of LLO, which needs to be further explored. The hypothesis that Vav3 might only be important in the response to high concentrations of the toxin goes in line with the fact that the gene encoding the Guanine Nucleotide Exchange Factor Vav3 emerged as a strong candidate involved in the response to PFTS, in a gain-of-function screen performed under lytic doses of LLO.

To overcome the limitations of this study we designed and proposed here a new experimental approach which should allow the analysis of Vav3-overexpressing cells in a more accurate way and avoiding the contribution of non-transfected cells in the sample. Additional investigation should be performed using Vav3-GFP variants that were constructed in the context of this dissertation and should allow to better study the role of Vav3 in the resistance to LLO intoxication and/or in the effect on PM recovery upon LLO-induced damage.

The evaluation of the involvement of Vav3 in response to high doses of LLO represent an additional challenge as discrimination between cell damage and cell death will be required.

BIBLIOGRAPHY

1. Peraro, M. D. & Van Der Goot, F. G. Pore-forming toxins: Ancient, but never really out of fashion. *Nat. Rev. Microbiol.* **14**, 77–92 (2016).
2. Los, F. C. O., Randis, T. M., Aroian, R. V & Ratner, A. J. Role of Pore-Forming Toxins in Bacterial Infectious Diseases. *Microbiol. Mol. Biol. Rev.* **77**, 173 LP – 207 (2013).
3. Gonzalez, M. R., Bischofberger, M., Pernot, L., Van Der Goot, F. G. & Frêche, B. Bacterial pore-forming toxins: The (w)hole story? *Cell. Mol. Life Sci.* **65**, 493–507 (2008).
4. Valeva, A. *et al.* Evidence that clustered phosphocholine head groups serve as sites for binding and assembly of an oligomeric protein pore. *J. Biol. Chem.* **281**, 26014–26021 (2006).
5. Gordon, V. M. *et al. Clostridium septicum* alpha toxin uses glycosylphosphatidylinositol-anchored protein receptors. *J. Biol. Chem.* **274**, 27274–27280 (1999).
6. Griffitts, J. S. *et al.* Glycolipids as receptors for *Bacillus thuringiensis* crystal toxin. *Science* **307**, 922–925 (2005).
7. Duncan, J. L. & Schlegel, R. Effect of streptolysin o on erythrocyte membranes, liposomes, and lipid dispersions: A protein-cholesterol interaction. *J. Cell Biol.* **67**, 160–173 (1975).
8. Tweten, R. K., Parker, M. W. & Johnson, A. E. The cholesterol-dependent cytolysins. *Curr. Top. Microbiol. Immunol.* **257**, 15–33 (2001).
9. Bradley, K. A., Mogridge, J., Mourez, M., Collier, R. J. & Young, J. A. Identification of the cellular receptor for anthrax toxin. *Nature* **414**, 225–229 (2001).
10. Scobie, H. M., Rainey, G. J. A., Bradley, K. A. & Young, J. A. T. Human capillary morphogenesis protein 2 functions as an anthrax toxin receptor. *Proc. Natl. Acad. Sci. U. S. A.* **100**, 5170–5174 (2003).
11. Saha, N. & Banerjee, K. K. Carbohydrate-mediated regulation of interaction of *Vibrio cholerae* hemolysin with erythrocyte and phospholipid vesicle. *J. Biol. Chem.* **272**, 162–167 (1997).
12. Iacovache, I., Bischofberger, M. & van der Goot, F. G. Structure and assembly of pore-forming proteins. *Curr. Opin. Struct. Biol.* **20**, 241–246 (2010).
13. Rudnick, S. T., Jost, B. H., Songer, J. G. & Billington, S. J. The gene encoding pyolysin, the

pore-forming toxin of *Arcanobacterium pyogenes*, resides within a genomic islet flanked by essential genes. *FEMS Microbiol. Lett.* **225**, 241–247 (2003).

14. Shannon, J. G., Ross, C. L., Koehler, T. M. & Rest, R. F. Characterization of anthrolysin O, the *Bacillus anthracis* cholesterol-dependent cytolysin. *Infect. Immun.* **71**, 3183–3189 (2003).
15. Sugimoto, N., Haque, A., Horiguchi, Y. & Matsuda, M. Botulinolysin, a thiol-activated hemolysin produced by *Clostridium botulinum*, inhibits endothelium-dependent relaxation of rat aortic ring. *Toxicon* **35**, 1011–1023 (1997).
16. Mitsui, N., Mitsui, K. & Hase, J. Purification and Some Properties of Tetanolysin. *Microbiol. Immunol.* **24**, 575–584 (1980).
17. Ragaliauskas, T. *et al.* Inerolysin and vaginolysin, the cytolysins implicated in vaginal dysbiosis, differently impair molecular integrity of phospholipid membranes. *Sci. Rep.* **9**, 1–11 (2019).
18. Frehel, C. *et al.* Capacity of ivanolysin O to replace listeriolysin O in phagosomal escape and in vivo survival of *Listeria monocytogenes*. *Microbiology* **149**, 611–620 (2003).
19. Popoff, M. R. Clostridial pore-forming toxins: Powerful virulence factors. *Anaerobe* **30**, 220–238 (2014).
20. Gekara, N. O., Jacobs, T., Chakraborty, T. & Weiss, S. The cholesterol-dependent cytolysin listeriolysin O aggregates rafts via oligomerization. *Cell. Microbiol.* **7**, 1345–1356 (2005).
21. Hamon, M. A., Ribet, D., Stavru, F. & Cossart, P. Listeriolysin O: The Swiss army knife of Listeria. *Trends Microbiol.* **20**, 360–368 (2012).
22. Radoshevich, L. & Cossart, P. *Listeria monocytogenes*: Towards a complete picture of its physiology and pathogenesis. *Nat. Rev. Microbiol.* **16**, 32–46 (2018).
23. Acheson, D. Special section: food safety. *Clin. Infect. Dis.* **31**, 127 (2000).
24. Crum, N. F. Update on *Listeria monocytogenes* infection. *Curr. Gastroenterol. Rep.* **4**, 287–296 (2002).
25. S. Schlech et al. - 1983 - Epidemic Listeriosis — Evidence for Transmission by Food. (198AD).
26. Nguyen, B. N., Peterson, B. N. & Portnoy, D. A. Listeriolysin O: A phagosome-specific cytolysin revisited. *Cell. Microbiol.* **21**, 1–12 (2019).
27. Camejo, A. *et al.* The arsenal of virulence factors deployed by *Listeria monocytogenes*

to promote its cell infection cycle. *Virulence* **2**, 379–394 (2011).

28. Painter, J. & Slutsker, L. Listeriosis in humans. in *Listeria, Listeriosis, and Food Safety, Third Edition* 85–110 (2007).
29. Rolhion, N. & Cossart, P. How the study of *Listeria monocytogenes* has led to new concepts in biology. *Future Microbiol.* **12**, 621–638 (2017).
30. de las Heras, A., Cain, R. J., Bielecka, M. K. & Vázquez-Boland, J. A. Regulation of Listeria virulence: PrfA master and commander. *Curr. Opin. Microbiol.* **14**, 118–127 (2011).
31. Gahan, C. G. M. & Hill, C. Gastrointestinal phase of *Listeria monocytogenes* infection. *J. Appl. Microbiol.* **98**, 1345–1353 (2005).
32. Cossart, P. & Kocks, C. The actin-based motility of the facultative intracellular pathogen *Listeria monocytogenes*. *Mol. Microbiol.* **13**, 395–402 (1994).
33. Gedde, M. M., Higgins, D. E., Tilney, L. G. & Portnoy, D. A. Role of listeriolysin O in cell-to-cell spread of *Listeria monocytogenes*. *Infect. Immun.* **68**, 999–1003 (2000).
34. Bonazzi, M., Lecuit, M. & Cossart, P. E-cadherin : From Bench to Bedside. 1–15 (2009).
35. Schnupf, P., Zhou, J., Varshavsky, A. & Portnoy, D. A. Listeriolysin O secreted by *Listeria monocytogenes* into the host cell cytosol is degraded by the N-end rule pathway. *Infect. Immun.* **75**, 5135–5147 (2007).
36. Köster, S. *et al.* Crystal structure of listeriolysin O reveals molecular details of oligomerization and pore formation. *Nature Communications* vol. 5 (2014).
37. Brito, C., Cabanes, D., Sarmento Mesquita, F. & Sousa, S. Mechanisms protecting host cells against bacterial pore-forming toxins. *Cell. Mol. Life Sci.* **76**, 1319–1339 (2019).
38. Brito, C. *et al.* Perfringolysin O-induced plasma membrane pores trigger actomyosin remodeling and endoplasmic reticulum redistribution. *Toxins (Basel).* **11**, (2019).
39. Birmingham, C. L. *et al. Listeria monocytogenes* evades killing by autophagy during colonization of host cells. *Autophagy* **3**, 442–451 (2007).
40. Yoshikawa, Y. *et al. Listeria monocytogenes* ActA-mediated escape from autophagic recognition. *Nat. Cell Biol.* **11**, 1233–1240 (2009).
41. Serrano Cardona, L. & Muñoz Mata, E. Paraninfo Digital. *Early Hum. Dev.* **83**, 1–11 (2013).
42. Hamon, M. A. *et al.* Histone modifications induced by a family of bacterial toxins. *Proc. Natl. Acad. Sci. U. S. A.* **104**, 13467–13472 (2007).
43. De Brito, O. M. & Scorrano, L. An intimate liaison: Spatial organization of the

endoplasmic reticulum-mitochondria relationship. *EMBO J.* **29**, 2715–2723 (2010).

44. Gareau, J. R. & Lima, C. D. The SUMO pathway: Emerging mechanisms that shape specificity, conjugation and recognition. *Nat. Rev. Mol. Cell Biol.* **11**, 861–871 (2010).
45. Ribet, D. *et al.* Europe PMC Funders Group *Listeria monocytogenes* impairs SUMOylation for efficient infection. **464**, 1192–1195 (2013).
46. Malet, J. K. *et al.* Rapid remodeling of the host epithelial cell proteome by the listeriolysin O (LLO) pore-forming toxin. *Mol. Cell. Proteomics* **17**, 1627–1636 (2018).
47. Dortet, L. *et al.* Recruitment of the major vault protein by inlk: A *Listeria monocytogenes* strategy to avoid autophagy. *PLoS Pathog.* **7**, (2011).
48. Stavru, F., Bouillaud, F., Sartori, A., Ricquier, D. & Cossart, P. *Listeria monocytogenes* transiently alters mitochondrial dynamics during infection. *Proc. Natl. Acad. Sci. U. S. A.* **108**, 3612–3617 (2011).
49. Stavru, F. & Cossart, P. Listeria infection modulates mitochondrial dynamics. *Commun. Integr. Biol.* **4**, 364–366 (2011).
50. Ribet, D. *et al. Listeria monocytogenes* impairs SUMOylation for efficient infection. *Nature* **464**, 1192–1195 (2010).
51. Horn, A. & Jaiswal, J. K. Cellular mechanisms and signals that coordinate plasma membrane repair. *Cell. Mol. Life Sci.* **75**, 3751–3770 (2018).
52. Mondal, A. K. *et al.* Structural basis and functional implications of the membrane pore-formation mechanisms of bacterial pore-forming toxins. *Adv. Exp. Med. Biol.* **1112**, 281–291 (2018).
53. Jimenez, A. J. & Perez, F. Plasma membrane repair: the adaptable cell life-insurance. *Curr. Opin. Cell Biol.* **47**, 99–107 (2017).
54. Andrews, N. W. & Corrotte, M. Plasma membrane repair. *Curr. Biol.* **28**, R392–R397 (2018).
55. Gekara, N. O. *et al.* The multiple mechanisms of Ca2+ signalling by listeriolysin O, the cholesterol-dependent cytolysin of *Listeria monocytogenes*. *Cell. Microbiol.* **9**, 2008–2021 (2007).
56. Andrews, N. W., Almeida, P. E. & Corrotte, M. Damage control: Cellular mechanisms of plasma membrane repair. *Trends Cell Biol.* **24**, 734–742 (2014).
57. Jimenez, A. J. & Perez, F. Physico-chemical and biological considerations for membrane wound evolution and repair in animal cells. *Semin. Cell Dev. Biol.* **45**, 2–9 (2015).

58. Gonzalez, M. R. *et al.* Pore-forming toxins induce multiple cellular responses promoting survival. *Cell. Microbiol.* **13**, 1026–1043 (2011).

59. Gonzalez, M. R. *et al.* Pore-forming toxins induce multiple cellular responses promoting survival. *Cell. Microbiol.* **13**, 1026–1043 (2011).

60. Wolfmeier, H. *et al.* Ca2+-dependent repair of pneumolysin pores: A new paradigm for host cellular defense against bacterial pore-forming toxins. *Biochim. Biophys. Acta - Mol. Cell Res.* **1853**, 2045–2054 (2014).

61. Tan, J. M. J. *et al.* An ATG16L1-dependent pathway promotes plasma membrane repair and limits *Listeria monocytogenes* cell-to-cell spread. *Nat. Microbiol.* **3**, 1472–1485 (2018).

62. McNeil, P. L. & Steinhardt, R. A. Loss, restoration, and maintenance of plasma membrane integrity. *J. Cell Biol.* **137**, 1–4 (1997).

63. Etxaniz, A., González-Bullón, D., Martín, C. & Ostolaza, H. Membrane repair mechanisms against permeabilization by pore-forming toxins. *Toxins (Basel).* **10**, (2018).

64. Gerke, V., Creutz, C. E. & Moss, S. E. Annexins: Linking Ca2+ signalling to membrane dynamics. *Nat. Rev. Mol. Cell Biol.* **6**, 449–461 (2005).

65. Boye, T. L. & Nylandsted, J. Annexins in plasma membrane repair. *Biol. Chem.* **397**, 961–969 (2016).

66. Potez, S. *et al.* Tailored protection against plasmalemmal injury by annexins with different Ca2+ sensitivities. *J. Biol. Chem.* **286**, 17982–17991 (2011).

67. Sierra, H., Cordova, M., Chen, C. S. J. & Rajadhyaksha, M. Confocal imaging-guided laser ablation of basal cell carcinomas: An ex vivo study. *J. Invest. Dermatol.* **135**, 612–615 (2015).

68. Charras, G. T. A short history of blebbing. *J. Microsc.* **231**, 466–478 (2008).

69. Charras, G. & Paluch, E. Blebs lead the way: How to migrate without lamellipodia. *Nat. Rev. Mol. Cell Biol.* **9**, 730–736 (2008).

70. Skočaj, M. *et al.* Characterisation of plasmalemmal shedding of vesicles induced by the cholesterol/sphingomyelin binding protein, ostreolysin A-mCherry. *Biochim. Biophys. Acta - Biomembr.* **1858**, 2882–2893 (2016).

71. Jimenez, A. J. *et al.* ESCRT machinery is required for plasma membrane repair. *Science (80-.).* **343**, (2014).

72. Romero, M. *et al.* Intrinsic repair protects cells from pore-forming toxins by microvesicle shedding. *Cell Death Differ.* **24**, 798–808 (2017).

73. Atanassoff, A. P. *et al.* Microvesicle Shedding and Lysosomal Repair Fulfill Divergent Cellular Needs during the Repair of Streptolysin O-Induced Plasmalemmal Damage. **9**, (2014).

74. Keyel, P. A. *et al.* Streptolysin O clearance through sequestration into blebs that bud passively from the plasma membrane. *J. Cell Sci.* **124**, 2414–2423 (2011).

75. Wickman, G. R. *et al.* Blebs produced by actin-myosin contraction during apoptosis release damage-associated molecular pattern proteins before secondary necrosis occurs. *Cell Death Differ.* **20**, 1293–1305 (2013).

76. Lee, K. *et al.* Enterocyte Purge and Rapid Recovery Is a Resilience Reaction of the Gut Epithelium to Pore-Forming Article Enterocyte Purge and Rapid Recovery Is a Resilience Reaction of the Gut Epithelium to Pore-Forming Toxin Attack. 1–15 (2016) doi:10.1016/j.chom.2016.10.010.

77. McNeil, P. L., Vogel, S. S., Miyake, K. & Terasaki, M. Patching plasma membrane disruptions with cytoplasmic membrane. *J. Cell Sci.* **113**, 1891–1902 (2000).

78. Bielecki, J., Youngman, P., Connelly, P. & Portnoy, D. A. Bacillus subtilis expressing a haemolysin gene from *Listeria monocytogenes* can grow in mammalian cells. *Nature* **345**, 175–176 (1990).

79. Steinhardt, R. A., Togo, T. & Krasieva, T. B. A Decrease in Membrane Tension Precedes Successful Cell-Membrane Repair. *Mol. Biol. Cell* **11**, 4339–4346 (2000).

80. Tam, C. *et al.* Exocytosis of acid sphingomyelinase by wounded cells promotes endocytosis and plasma membrane repair. *J. Cell Biol.* **189**, 1027–1038 (2010).

81. Castro-Gomes, T., Corrotte, M., Tam, C. & Andrews, N. W. Plasma membrane repair is regulated extracellularly by proteases released from lysosomes. *PLoS One* **11**, 1–26 (2016).

82. Michelet, X. *et al.* Lysosome-Mediated Plasma Membrane Repair Is Dependent on the Small GTPase Arl8b and Determines Cell Death Type in Mycobacterium tuberculosis Infection. (2020) doi:10.4049/jimmunol.1700829.

83. Chakrabarti, S. *et al.* Impaired membrane resealing and autoimmune myositis in synaptotagmin VII-deficient mice. *J. Cell Biol.* **162**, 543–549 (2003).

84. Defour, A. *et al.* Dysferlin regulates cell membrane repair by facilitating injury-triggered

acid sphingomyelinase secretion. *Cell Death Dis.* **5**, e1306-11 (2014).

85. Czibener, C. *et al.* Ca2+ and synaptotagmin VII-dependent delivery of lysosomal membrane to nascent phagosomes. *J. Cell Biol.* **174**, 997–1007 (2006).
86. Skalman, L. N., Holst, M. R., Larsson, E. & Lundmark, R. Plasma membrane damage caused by listeriolysin O is not repaired through endocytosis of the membrane pore. *Biol. Open* **7**, (2018).
87. Bianco, F. *et al.* Acid sphingomyelinase activity triggers microparticle release from glial cells. *EMBO J.* **28**, 1043–1054 (2009).
88. Sousa, S. *et al.* Src, cortactin and Arp2/3 complex are required for E-cadherin-mediated internalization of Listeria into cells. *Cell. Microbiol.* **9**, 2629–2643 (2007).
89. Almeida, M. T. *et al.* Src-dependent tyrosine phosphorylation of non-muscle myosin heavy chain-IIA restricts *Listeria monocytogenes* cellular infection. *J. Biol. Chem.* **290**, 8383–8395 (2015).
90. Cruz, R. *et al.* Epithelial keratins modulate cMet expression and signaling and promote InlB-mediated *Listeria monocytogenes* infection of HeLa cells. *Front. Cell. Infect. Microbiol.* **8**, (2018).
91. Costa, A. C., Carvalho, F., Cabanes, D. & Sousa, S. Stathmin recruits tubulin to *Listeria monocytogenes*-induced actin comets and promotes bacterial dissemination. *Cell. Mol. Life Sci.* **76**, 961–975 (2019).
92. Mesquita, F. S. *et al.* Endoplasmic reticulum chaperone Gp96 controls actomyosin dynamics and protects against pore-forming toxins. *EMBO Rep.* **18**, 303–318 (2017).
93. Chen, L. *et al.* Transposon activation mutagenesis as a screening tool for identifying resistance to cancer therapeutics. *BMC Cancer* **13**, 1 (2013).
94. Kawakami, K., Largaespada, D. A. & Ivics, Z. Transposons As Tools for Functional Genomics in Vertebrate Models. *Trends Genet.* **33**, 784–801 (2017).
95. Rojas, A. M., Fuentes, G., Rausell, A. & Valencia, A. The Ras protein superfamily: Evolutionary tree and role of conserved amino acids. *J. Cell Biol.* **196**, 189–201 (2012).
96. Vega, F. M. & Ridley, A. J. Rho GTPases in cancer cell biology. *FEBS Lett.* **582**, 2093–2101 (2008).
97. Van Aelst, L. & D'Souza-Schorey, C. Rho GTPases and signaling networks. *Genes Dev.* **11**, 2295–2322 (1997).
98. Bement, W. M., Miller, A. L. & Von Dassow, G. Rho GTPase activity zones and transient

contractile arrays. *BioEssays* **28**, 983–993 (2006).

99. Haga, R. B. & Ridley, A. J. Rho GTPases: Regulation and roles in cancer cell biology. *Small GTPases* **7**, 207–221 (2016).
100. Cook, D. R., Rossman, K. L. & Der, C. J. Rho guanine nucleotide exchange factors: Regulators of Rho GTPase activity in development and disease. *Oncogene* **33**, 4021–4035 (2014).
101. Bustelo, X. R. Understanding Rho/Rac biology in T-cells using animal models. *BioEssays* **24**, 602–612 (2002).
102. Govek, E. E., Newey, S. E. & Van Aelst, L. The role of the Rho GTPases in neuronal development. *Genes Dev.* **19**, 1–49 (2005).
103. Hall, A. Rho family GTPases. *Biochem. Soc. Trans.* **40**, 1378–1382 (2012).
104. Cherfils, J. & Zeghouf, M. Regulation of small GTPases by GEFs, GAPs, and GDIs. *Physiol. Rev.* **93**, 269–309 (2013).
105. Duman, J. G., Mulherkar, S., Tu, Y. K., X. Cheng, J. & Tolias, K. F. Mechanisms for spatiotemporal regulation of Rho-GTPase signaling at synapses. *Neurosci. Lett.* **601**, 4–10 (2015).
106. Song, S. *et al.* Small GTPases: Structure, biological function and its interaction with nanoparticles. *Asian J. Pharm. Sci.* **14**, 30–39 (2019).
107. Hornstein, I., Alcover, A. & Katzav, S. Vav proteins, masters of the world of cytoskeleton organization. *Cell. Signal.* **16**, 1–11 (2004).
108. Bustelo, X. R. Vav proteins, adaptors and cell signaling. *Oncogene* **20**, 6372–6381 (2001).
109. Bustelo, X. R. & Dosil, M. Vav Family. in *Encyclopedia of Signaling Molecules* (ed. Choi, S.) 5892–5906 (Springer International Publishing, 2018). doi:10.1007/978-3-319-67199-4_513.
110. Ilan, L. & Katzav, S. Human Vav1 expression in hematopoietic and cancer cell lines is regulated by c-Myb and by CpG methylation. *PLoS One* **7**, 1–11 (2012).
111. Bustelo, X. R. Regulatory and Signaling Properties of the Vav Family. *Mol. Cell. Biol.* **20**, 1461–1477 (2000).
112. Zeng, L. *et al.* Vav3 Mediates Receptor Protein Tyrosine Kinase Signaling, Regulates GTPase Activity, Modulates Cell Morphology, and Induces Cell Transformation. *Mol. Cell. Biol.* **20**, 9212–9224 (2000).

113. Bustelo, X. R., Sauzeau, V. & Berenjeno, I. M. GTP-binding proteins of the Rho Rac family. **29**, 356–370 (2007).

114. López-Lago, M., Lee, H., Cruz, C., Movilla, N. & Bustelo, X. R. Tyrosine Phosphorylation Mediates Both Activation and Downmodulation of the Biological Activity of Vav. *Mol. Cell. Biol.* **20**, 1678–1691 (2000).

115. Moores, S. L. *et al.* Vav Family Proteins Couple to Diverse Cell Surface Receptors. *Mol. Cell. Biol.* **20**, 6364–6373 (2000).

116. Zugaza, J. L. *et al.* Structural determinants for the biological activity of Vav proteins. *J. Biol. Chem.* **277**, 45377–45392 (2002).

117. Fischer, K. D., Tedford, K. & Penninger, J. M. Vav links antigen-receptor signaling to the actin cytoskeleton. *Semin. Immunol.* **10**, 317–327 (1998).

118. Bustelo, X. R. Vav family exchange factors: An integrated regulatory and functional view. *Small GTPases* **5**, (2014).

119. Movilla, N. & Bustelo, X. R. Biological and Regulatory Properties of Vav-3, a New Member of the Vav Family of Oncoproteins. *Mol. Cell. Biol.* **19**, 7870–7885 (1999).

120. Várni, P. *et al.* Selective cellular effects of overexpressed pleckstrin-homology domains that recognize Ptdlns(3,4,5)P3 suggest their interaction with protein binding partners. *J. Cell Sci.* **118**, 4879–4888 (2005).

121. Swat, W. & Fujikawa, K. The Vav family: At the crossroads of signaling pathways. *Immunol. Res.* **32**, 259–265 (2005).

122. Hilfenhaus, G. *et al.* Vav3-induced cytoskeletal dynamics contribute to heterotypic properties of endothelial barriers. *J. Cell Biol.* **217**, 2813–2830 (2018).

123. Rao, S. *et al.* A novel nuclear role for the Vav3 nucleotide exchange factor in androgen receptor coactivation in prostate cancer. *Oncogene* **31**, 716–727 (2012).

124. Glomski, I. J., Gedde, M. M., Tsang, A. W., Swanson, J. A. & Portnoy, D. A. The *Listeria monocytogenes* hemolysin has an acidic pH optimum to compartmentalize activity and prevent damage to infected host cells. *J. Cell Biol.* **156**, 1029–1038 (2002).

125. Schindelin, J. *et al.* Fiji: an open-source platform for biological-image analysis. *Nat. Methods* **9**, 676–682 (2012).

126. Lyons, L. S. & Burnstein, K. L. Vav3, a Rho GTPase guanine nucleotide exchange factor, increases during progression to androgen independence in prostate cancer cells and potentiates androgen receptor transcriptional activity. *Mol. Endocrinol.* **20**, 1061–1072

(2006).

127. Pinheiro, J. *et al. Listeria monocytogenes* encodes a functional ESX-1 secretion system whose expression is detrimental to in vivo infection. *Virulence* **8**, 993–1004 (2017).
128. Babiychuk, E. B. & Draeger, A. Defying death: Cellular survival strategies following plasmalemmal injury by bacterial toxins. *Semin. Cell Dev. Biol.* **45**, 39–47 (2015).
129. Seveau, S. Multifaceted activity of listeriolysin O, the cholesterol-dependent cytolysin of *Listeria monocytogenes*. *Subcell. Biochem.* **80**, 161–195 (2014).
130. Cassidy, S. K. B. & O'Riordan, M. X. D. More than a pore: The cellular response to cholesterol-dependent cytolysins. *Toxins (Basel).* **5**, 618–636 (2013).
131. Draeger, A., Schoenauer, R., Atanassoff, A. P., Wolfmeier, H. & Babiychuk, E. B. Dealing with damage: plasma membrane repair mechanisms. *Biochimie* **107 Pt A**, 66–72 (2014).
132. Salhia, B. *et al.* The guanine nucleotide exchange factors trio, Ect2, and Vav3 mediate the invasive behavior of glioblastoma. *Am. J. Pathol.* **173**, 1828–1838 (2008).
133. Dong, Z. *et al.* Vav3 Oncogene Is Overexpressed and Regulates Cell Growth and Androgen Receptor Activity in Human Prostate Cancer. *Mol. Endocrinol.* **20**, 2315–2325 (2006).
134. Kondo, T., Oka, T., Sato, H., Shinnou, Y. & Washio, K. Accumulation of aberrant CpG hypermethylation by Helicobacter pylori infection promotes development. *Int. J. Oncol.* **35**, 547–557 (2009).
135. Bouvet, F. *et al.* Defective membrane repair machinery impairs survival of invasive cancer cells. *Sci. Rep.* **10**, 1–16 (2020).